

Synthesis of Bis(phosphino)silyl Pincer-Supported Iron Hydrides for the Catalytic Hydrogenation of Alkenes

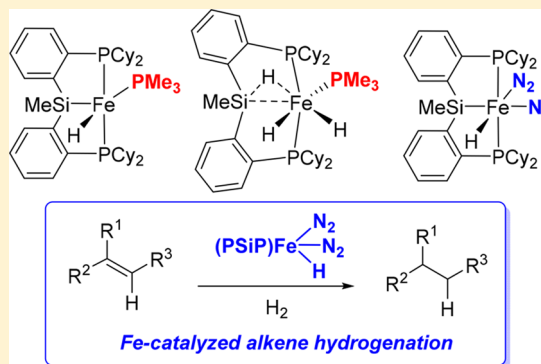
Luke J. Murphy,[†] Michael J. Ferguson,^{‡,b} Robert McDonald,^{‡,b} Michael D. Lumsden,[†] and Laura Turculet^{*,†,b}

[†]Department of Chemistry, Dalhousie University, 6274 Coburg Road, P.O. Box 15000, Halifax, Nova Scotia, Canada B3H 4R2

[‡]X-Ray Crystallography Laboratory, Department of Chemistry, University of Alberta, Edmonton, Alberta, Canada T6G 2G2

S Supporting Information

ABSTRACT: The synthesis and characterization of Fe pincer complexes supported by a bis(phosphino)silyl (PSiP) ligand are described. While four-coordinate species of the type (PSiP)FeX (X = halide) proved challenging to access, examples of five-coordinate (PSiP)Fe(II) and (PSiP)Fe(I) species were prepared and crystallographically characterized. In studying the reactivity of such (PSiP)Fe precursors, a variety of iron hydride species were observed and characterized, and interconversion among such complexes facilitated by the coordination of N₂ was noted. The structures and spectroscopic features of several such diamagnetic Fe(II) hydrides were elucidated, including that of a unique and highly stable η^2 -(Si–H)Fe(II) dihydride complex. A surrogate for a low coordinate (PSiP)FeH species in the form of its bis(dinitrogen) adduct was found to be an effective precatalyst for the direct hydrogenation of alkenes, including various mono- and disubstituted aliphatic alkenes, as well as a trisubstituted example. Esters and ethers were found to be well-tolerated by the catalyst, and alkyne hydrogenation was also demonstrated.

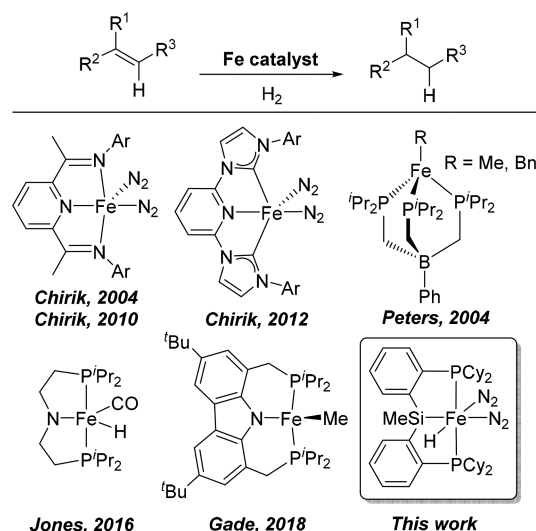


1. INTRODUCTION

The hydrogenation of alkenes is one of the most important and widely applied chemical transformations known, with applications ranging from the synthesis of fine chemicals to the processing of petrochemicals, and it is routinely employed on large scales.¹ Traditionally, alkene hydrogenation processes have been dominated by the use of transition metal catalysts, most often of the platinum group metals. However, there has been recent success in the development of systems utilizing more abundant and less costly first-row transition metals,² particularly cobalt,³ though well-defined examples of readily accessible and easily handled homogeneous catalysts with high activity and functional group tolerance still remain relatively scarce, especially in the case of iron. Yet iron is in many ways an ideal metal to employ in catalysis,⁴ due primarily to its low cost, comparatively low toxicity, and high abundance.

In 2004, Chirik and co-workers⁵ developed an Fe-based alkene hydrogenation catalyst, (IPr)PDI)Fe(N₂)₂, supported by a bis(imino)pyridinyl scaffold (Chart 1). The discovery of this catalyst marked an important step forward in the field of Fe-catalyzed olefin hydrogenation, as prior to this the only examples of such a transformation involved the use of Fe(CO)₅ as a catalyst at high temperature and pressure or under photocatalytic conditions.^{3f,6} Around the same time Peters and co-workers⁷ reported alkene hydrogenation catalyzed by a tris(phosphino)borato-supported Fe complex

Chart 1. Fe Catalysts for the Hydrogenation of Alkenes



under mild conditions (1–4 atm H₂, 23 °C), albeit at higher (10 mol %) catalyst loadings.

Received: November 3, 2018

In Chirik's initial Fe system,⁵ (ⁱPrPDI)Fe(N₂)₂ was found to hydrogenate a variety of terminal, internal, and *gem*-disubstituted alkenes under very mild conditions and at low catalyst loadings. However, trisubstituted alkenes could not be hydrogenated under these conditions. In a subsequent report⁸ functional group tolerance in the catalytic system was investigated, with examples of amino, ether, ketone, and ester functionalized alkenes undergoing chemoselective alkene hydrogenation under varying conditions (some requiring elevated temperatures or a higher catalyst loading). However, the authors also identified C–O bond cleavage of ethers and esters by the catalyst as a problematic side-reaction resulting in catalyst deactivation if substrate and catalyst were not kept frozen at liquid N₂ temperature until H₂ addition.⁹ More recently, investigations into ligand modifications of the original ligand structure¹⁰ ultimately led to a bis(arylimidazol-2-ylidene)pyridinyl scaffold (Chart 1).¹¹ Such (^RCNC)Fe(N₂)₂ (R = Me, Mes) complexes were found to be active for the hydrogenation of a handful of trisubstituted alkenes and even a tetrasubstituted alkene (2,3-dimethyl-1H-indene, 60–68% conversion over 48 h).^{11b}

In other recent contributions, monoanionic PNP pincer ligation has been explored in the context of Fe-catalyzed alkene hydrogenation. Jones and co-workers¹² reported the hydrogenation of styrene derivatives using a (PNP)Fe(H)(CO) precatalyst (PNP=N(CH₂CH₂P^tPr₂)₂, Chart 1). While various styrenes, including substrates featuring ester and nitrile substitution on the arene ring, were reduced with high conversion and selectivity, nonpolar aliphatic alkenes such as 1-hexene were not hydrogenated, even at increased temperature and pressure. DFT calculations support a bifunctional mechanism involving stepwise transfer of Fe-hydride from (PNHP)Fe(H)₂(CO) to the C=C bond, followed by proton transfer from the N–H in the pincer backbone. This mechanism is in agreement with the observed rate dependence of the reaction on the polarity of the C=C bond. Subsequently, Gade and co-workers¹³ reported high-spin, bis(phosphino)pyrrole (PNP)Fe(alkyl) complexes that functioned as precatalysts for alkene hydrogenation (Chart 1). Secondary aliphatic alkenes, such as 2-pentene and 2-hexene, were hydrogenated effectively, while *trans*-stilbene only reached 34% conversion after 72 h, and the tetrasubstituted alkene 2,3-dimethylbut-2-ene proved unreactive.

The use of a bis(anthracene) metalate of iron, as well as other related arene metalate iron complexes, for catalytic alkene hydrogenation was also recently explored.¹⁴ However, outside of high conversions for a select number of terminal alkenes (styrene derivatives, 1-octene, and 1-dodecene) catalytic performance was quite poor for these systems, while related cobalt complexes were found to be more active. The hydrogenation of α,β -unsaturated carbonyl compounds by an Fe(II)/EDTA catalyst has also been reported.¹⁵ Outside the realm of well-defined homogeneous catalysts, recent examples of effective Fe-hydrogenation catalysts include MOF-supported species,¹⁶ as well as systems involving *in situ* generated Fe hydride clusters and Fe nanoparticles. In one such report from Jacobi von Wangelin and co-workers,¹⁷ a combination of 5 mol % FeCl₃ with 5–10 mol % LiAlH₄ was employed to generate the catalyst species. The substrate scope featured predominantly terminal or disubstituted alkenes, with a trisubstituted alkene (1-phenylcyclohexene) giving <20% conversion. The authors proposed a homogeneous catalytic cycle at the onset of catalysis, giving way to insoluble Fe(0) species that exhibit

lower catalytic activity. A second report from this group¹⁸ invokes generation of Fe hydride nanoclusters upon reaction of Fe[N(SiMe₃)₂]₂ (5 mol %) with DIBAL-H (10 mol %), which enables a broad variety of alkene hydrogenations, with terminal, disubstituted, trisubstituted, and even several tetrasubstituted alkenes hydrogenated in moderate to excellent yields.

While the above examples illustrate significant advances in the field of Fe-catalyzed alkene hydrogenation, the identification of new ligands that are capable of supporting effective Fe catalysts for alkene hydrogenation remains an important goal. In particular, further effort is needed to develop catalysts that not only exhibit functional group tolerance but are also easily handled and not susceptible to decomposition in the presence of substrate. Investigation into the stoichiometric chemistry of ligand-supported Fe hydride complexes is key to this effort, as such Fe hydride complexes are expected to be vital intermediates in a catalytic cycle where alkene coordination and subsequent migratory insertion likely represent fundamental mechanistic steps. In this regard, fundamental studies examining the role of ancillary ligation in supporting low-coordinate Fe hydride complexes are also important, as the steric requirements for the coordination of weakly donating or sterically congested alkenes must be suitably balanced with the electronic requirements for the activation and eventual reduction of an unsaturated substrate at the Fe center.

Our group has investigated the utility of tridentate bis(phosphino)silyl (PSiP) ligation for group 8, 9, and 10 transition metals, with the aim of uncovering new routes to challenging bond activation processes as well as catalytic applications.^{19,20} In this regard we have identified routes to the C–H activation of benzene,²¹ the N–H activation of ammonia,²² in addition to catalytic reduction of CO₂ to methane.²³ Most recently we have become interested in exploring the behavior of PSiP ligand scaffolds in conjunction with the more abundant, and consequently less costly, first-row transition metals, and we have demonstrated a highly selective reduction of CO₂ to the formaldehyde level catalyzed by a (PSiP)Ni complex.²⁴ We have also pursued the synthesis and reactivity of (PSiP)Co species, including their application in alkene hydrogenation catalysis.²⁵ Comparatively, (PSiP)Fe chemistry is remarkably underexplored, with three reports appearing in the literature to date, in which only saturated 18-electron Fe(II) complexes for use outside of alkene hydrogenation are described.²⁶ Inspired by the progress made to date regarding homogeneous Fe-catalyzed alkene hydrogenation (*vide supra*), we sought to prepare an active Fe catalyst based on the PSiP ligand scaffold, in anticipation that the strong *trans*-influence of the anionic silyl donor would promote generation of a reactive, low-coordinate Fe species poised to undergo the necessary steps to facilitate such a transformation.

Herein we report significant progress in the field of (PSiP)Fe chemistry, including the application of (PSiP)Fe(II)-hydride species in alkene hydrogenation catalysis. In the course of these studies, (PSiP)Fe-hydride chemistry has been explored in detail, including the synthesis of a unique η^2 -silane complex of an Fe(II) dihydride, as well as a bis(dinitrogen) Fe(II) hydride (inset, Chart 1), which was found to be an isolable and easily handled precatalyst for the hydrogenation of a variety of alkenes.

2. RESULTS AND DISCUSSION

Synthesis of (PSiP)Fe-Halide Complexes. Previous efforts to access (PSiP)Fe chemistry, as reported by the Sun, Iwasawa, and Nishibayashi groups, have focused on the synthesis of saturated, 18-electron derivatives of the form (R-PSiP^{R'})FeH(PMe₃)(L) (R-PSiP^{R'} = κ^3 -(2-R₂PC₆H₄)₂SiR'; R = Cy, Ph; R' = Me, Ph; L = PMe₃, N₂).^{26a,c} In efforts to uncover new and relevant reactivity toward substrate molecules featuring E-H bonds (e.g., H₂, silanes, boranes), we first sought to generate four-coordinate Fe(II) complexes of the form (Cy-PSiP^{Me})FeX (X = halide). While examples of Co analogues of this type have been successfully isolated and characterized,^{20i,25,26c} to date no evidence for the corresponding Fe complexes has been observed.

In an analogous fashion to the preparation of (R-PSiP^{Me})-CoX,^{20i,25,26c} compounds of the form (Cy-PSiP^{Me})FeX were targeted by treatment of the tertiary silane (Cy-PSiP^{Me})H with an FeX₂ precursor and base. While many attempts were made to induce Si-H metalation by varying the base (a broad range of bases were studied in this regard, including amines) and FeX₂ source, these attempts were largely unsuccessful, as the resulting paramagnetic products proved difficult to isolate in pure form. In some cases, samples of crystalline material obtained from such reactions revealed the formation of Fe(I) and Fe(III) species, implicating undesired one-electron redox processes in the observed reactivity. In one case, a minute amount of X-ray quality crystals of monomeric, four-coordinate (Cy-PSiP^{Me})FeBr (**1-Br**, Figure S1) were obtained from treatment of (Cy-PSiP^{Me})H with FeBr₂ and one equiv of MeMgBr at low temperature. While the obtained crystals and corresponding X-ray data likely represent only a small portion of the resultant product mixture, the observations nonetheless support the feasibility of complexes of the desired formulation. Details of these attempts, including X-ray crystal structures obtained in the course of our investigations, are summarized in the Supporting Information.

As complexes of the type (Cy-PSiP^{Me})FeX proved challenging to isolate, stabilization of these reactive compounds with an additional ligand was pursued. In previous reports by Sun,^{26a} as well as Nihibayashi and Iwasawa,^{26c} (PSiP)M (M = Fe, Co, Ni) complexes were accessed through the use of the zerovalent M(PMe₃)₄ starting materials, and thus the resulting saturated complexes all feature one or two equiv PMe₃ bound to the metal center. With this in mind, we treated a mixture of (Cy-PSiP^{Me})H, FeCl₂(THF)_{1.5} and one equiv PMe₃ with BnMgCl at -35 °C (Scheme 1). The five-coordinate Fe(II) complex (Cy-PSiP^{Me})Fe(PMe₃)Cl (**2·PMe₃**) was obtained as an analytically pure orange solid in 94% yield by this route. Use of CO (1 atm) in place of PMe₃ generated the dicarbonyl complex **2·(CO)₂**.

Solution magnetic moment measurements for **2·PMe₃** (Evans method, benzene-*d*₆, 300 K) resulted in a calculated μ_{eff} value of 3.0 μ_{B} (S = 1 ground state). The solid state structure of **2·PMe₃** (Figure 1) confirms the formulation of this complex as a 16-electron PMe₃ adduct that features distorted trigonal bipyramidal coordination geometry at iron with κ^3 -coordination of the PSiP ligand. The pincer ligand phosphino donors and the PMe₃ ligand are bound in the equatorial plane, while Si and Cl take up the axial positions. The related diamagnetic five-coordinate Ru complex (Cy-PSiP^{Me})Ru(PMe₃)Cl adopts a slightly different geometry in the solid state, with one pincer ligand phosphino donor and

Scheme 1. Synthetic Routes for the Preparation of **2·PMe₃** and **2·(CO)₂**

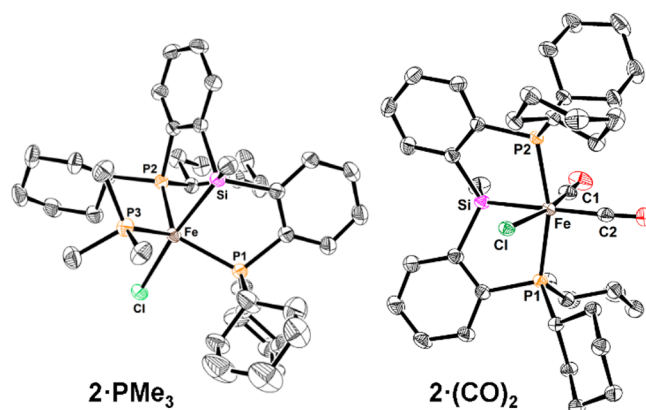
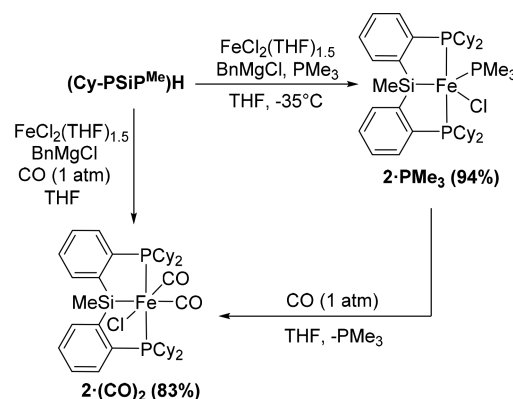


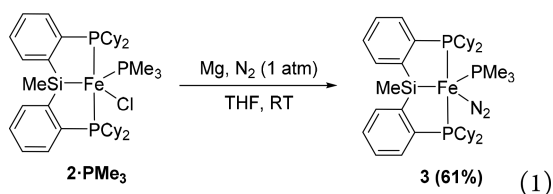
Figure 1. Crystallographically determined structures of **2·PMe₃** (left) and **2·(CO)₂** (right) with thermal ellipsoids shown at the 50% probability level (in each case, one of two crystallographically independent molecules is shown); hydrogen atoms have been omitted for clarity. Selected interatomic distances (Å) and angles (deg): for **2·PMe₃** Fe-Cl 2.2731(6), Fe-P1 2.23224(6), Fe-P2 2.3346(6), Fe-P3 2.3113(6), Fe-Si 2.3436(6), Cl-Fe-Si 173.20(2), P1-Fe-P2 122.82(2), P1-Fe-P3 121.93(2), P2-Fe-P3 110.38(2); for **2·(CO)₂** Fe-Cl 2.3435(4), Fe-P1 2.2786(4), Fe-P2 2.2761(4), Fe-Si 2.3284(5), Fe-C1 1.7228(17), Fe-C2 1.8203(16), O1-C1 1.159(2), O2-C2 1.145(2), Cl-Fe-Cl 167.71(5), P1-Fe-P2 162.500(17), Si-Fe-C2 173.93(5).

the PMe₃ ligand bound in the axial positions of a distorted trigonal bipyramidal structure.²⁷ Complex **2·PMe₃** is also closely related in structure to the tris(phosphino)silyl iron chloride complexes (Si^RP₃)FeCl (Si^RP₃ = κ^4 -(2-R₂PC₆H₄)₃Si; R = Ph or ⁱPr) prepared by Peters and co-workers,²⁸ which also feature slightly distorted trigonal bipyramidal geometry in the solid state and exhibit similar μ_{eff} values ($\mu_{\text{eff}} = 2.9 \mu_{\text{B}}$ and 3.3 μ_{B} for R = Ph and ⁱPr, respectively).

Complex **2·PMe₃** is the first example of an isolable, electronically unsaturated (PSiP)Fe complex. While similarities exist between **2·PMe₃** and related iron complexes prepared by Peters and co-workers that feature tetradentate tris-(phosphino)silyl ligation, the use of a tridentate ligand herein allows for potential dissociation or displacement of PMe₃ from the metal center, which may provide access to reactive low-coordinate iron species more readily. For example, exposure of a THF solution of **2·PMe₃** to an atmosphere of CO led to displacement of the PMe₃ ligand and clean conversion to the dicarbonyl complex **2·(CO)₂** (Scheme 1). Complex **2·(CO)₂** is

diamagnetic and forms as a single C_s -symmetric isomer in solution, as indicated by the presence of a single $^{31}\text{P}\{^1\text{H}\}$ NMR resonance at 86.2 ppm. The solid state structure of $2\cdot(\text{CO})_2$ (Figure 1) and the presence of two νCO IR stretches (1969, 1909 cm^{-1}), are consistent with the proposed formulation for this complex. The 6-coordinate complex features octahedral coordination geometry, with $\text{mer-}\kappa^3$ -coordination of the PSiP ligand.

Reduction of $2\cdot\text{PMe}_3$. Having previously observed evidence for redox processes involving putative $(\text{Cy-PSiP}^{\text{Me}})\text{-FeX}$ species, we considered that $2\cdot\text{PMe}_3$ might undergo a more controlled single-electron reduction to a corresponding Fe(I) complex. Although the +1 oxidation state is not common for iron, there are several well-characterized examples of Fe(I) complexes that have been previously reported, including related tris(phosphino)silyl species prepared by Peters and co-workers.²⁸ While Co(I) complexes of the form $(\text{R-PSiP}^{\text{Me}})\text{Co}(\text{PMe}_3)(\text{N}_2)$ have been synthesized and applied toward N_2 reduction^{26c} and alkene hydrogenation catalysis,²⁵ thus far there have been no well-defined examples of analogous five-coordinate PSiP-supported Fe(I) complexes. Such (PSiP)-Fe(I) complexes could be susceptible to oxidative addition reactions of E-H bonds, leading to Fe(III) species of the type $(\text{PSiP})\text{Fe}(\text{PMe}_3)(\text{E})(\text{H})$. Toward this end, a solution of $2\cdot\text{PMe}_3$ in THF was stirred with excess magnesium overnight under a N_2 atmosphere, leading to the formation of the desired paramagnetic complex $(\text{Cy-PSiP}^{\text{Me}})\text{Fe}(\text{PMe}_3)(\text{N}_2)$ (**3**; $\mu_{\text{eff}} = 1.9 \mu_{\text{B}}$, $S = 1/2$), which was isolated as a yellow solid in 61% yield (eq 1).



As in the case of $2\cdot\text{PMe}_3$, and the Co(I) analogue $(\text{Cy-PSiP}^{\text{Me}})\text{Co}(\text{PMe}_3)(\text{N}_2)$, the solid state structure of **3** (Figure 2) features trigonal bipyramidal coordination geometry at the iron center, with κ^3 -coordination of the PSiP ligand. The pincer ligand phosphino donors and the PMe_3 ligand are bound in the equatorial plane, while Si and N_2 take up the axial positions. The structure of **3** is also similar to that of $(\text{Si}^{\text{IPr}}\text{P}_3)\text{Fe}(\text{N}_2)$ reported by Peters and co-workers.²⁸ The N–N bond distance of 1.119(2) Å in **3** is elongated relative to that of 1.065(5) Å observed for $(\text{Si}^{\text{IPr}}\text{P}_3)\text{Fe}(\text{N}_2)$, which suggests increased electron backdonation from the iron center to the N_2 ligand (cf. N–N bond length of 1.0975 Å for free N_2). However, the νNN stretching frequency of 2011 cm^{-1} observed for **3** is nearly identical to the value of 2008 cm^{-1} obtained for $(\text{Si}^{\text{IPr}}\text{P}_3)\text{Fe}(\text{N}_2)$, indicating minimal electronic differences between the two complexes (cf. $\nu\text{NN} = 2331 \text{ cm}^{-1}$ for free N_2). As such, the N_2 ligand in **3** is best described as weakly activated.²⁹

PMe_3 Adducts of Fe(II)–Hydride Complexes. Having successfully reduced $2\cdot\text{PMe}_3$ to an Fe(I) species, the reactivity of **3** was first probed with respect to oxidative addition of E–H bonds. While in most cases (e.g. H_2 , PhSiH_3 , $\text{H}_3\text{N}\cdot\text{BH}_3$, $\text{HC}\equiv\text{CPh}$) evidence of a reaction was observed (based on color change) over the course of ca. 18 h at room temperature, most of these reactions led to the formation of complicated

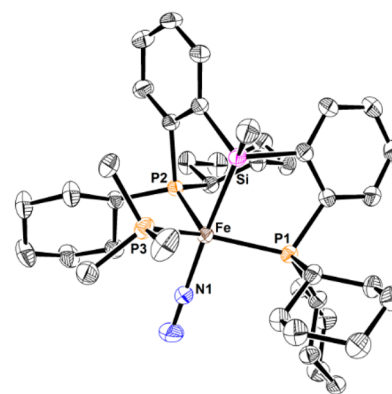
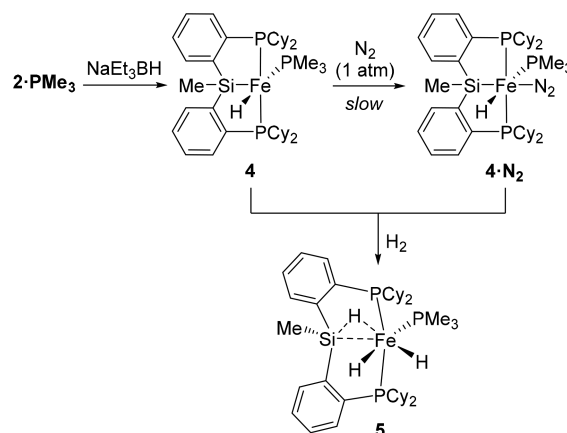


Figure 2. Crystallographically determined structure of **3** with thermal ellipsoids shown at the 50% probability level; hydrogen atoms have been omitted for clarity. Selected interatomic distances (Å) and angles (deg) for **3** (one of two crystallographically independent molecules): Fe–P1 2.2845(4), Fe–P2 2.2878(5), Fe–P3 2.2253(5), Fe–Si 2.3145(5), Fe–N1 1.8191(15), N1–N2 1.119(2), Si–Fe–N1 177.17(5), P1–Fe–P2 118.122(18), P1–Fe–P3 135.000(19), P2–Fe–P3 103.155(18).

paramagnetic product mixtures from which no pure material could be isolated. In select cases, the formation of a variety of distinct iron hydride species, including $(\text{Cy-PSiP}^{\text{Me}})\text{Fe}(\text{PMe}_3)(\text{N}_2)\text{H}$ (**4·N₂**), which has been previously reported by Nishibayashi, Iwasawa, and co-workers,^{26c} was observed. A description of these observations is included in the Supporting Information. As these hydride species were typically formed as mixtures by what often appeared to be complex mechanisms, the preparation of iron hydride species by more direct routes was pursued.

Toward this end, $2\cdot\text{PMe}_3$ was treated with one equiv NaEt_3BH under an N_2 atmosphere. Monitoring of this reaction mixture by ^1H and $^{31}\text{P}\{^1\text{H}\}$ NMR spectroscopy revealed the formation of a hydride complex formulated as $(\text{Cy-PSiP}^{\text{Me}})\text{Fe}(\text{PMe}_3)\text{H}$ (**4**, Scheme 2). Complex **4** gives rise to a Fe–H ^1H

Scheme 2. Synthesis of PMe_3 Adducts of Fe(II)–Hydride Complexes



NMR resonance at -18.53 ppm (td, $^2J_{\text{PH}} = 64.2$ Hz, $^2J_{\text{PH}} = 24.0$ Hz), as well as $^{31}\text{P}\{^1\text{H}\}$ NMR resonances at 90.0 (d, $^2J_{\text{PP}} = 55$ Hz) and 3.6 (t, $^2J_{\text{PP}} = 55$ Hz) ppm, assigned to the pincer phosphino donors and PMe_3 , respectively. The IR spectrum of **4** does not feature a band corresponding to the νNN stretch of coordinated N_2 . These spectroscopic signatures are distinct

from those reported for $4 \cdot N_2$ (1H NMR: -14.84 ppm Fe-H; $^{31}P\{^1H\}$ NMR: 84.8 PSiP, 11.5 ppm PM_e_3 ; $\nu_{NN} = 2041$ cm^{-1}).^{26c} In their report on the preparation of $4 \cdot N_2$ (accessed directly from reaction of (Cy-PSiP^{Me})H with $Fe(PMe_3)_4$) Nishibayashi and Iwasawa do not report N_2 loss from $4 \cdot N_2$, which suggests that the latter complex corresponds to a thermodynamic product from which N_2 loss is not facile. We observed that while complex **4** was formed as the major product from the reaction of $2 \cdot PM_e_3$ with $NaEt_3BH$, **4** coordinates N_2 over time to form trace $4 \cdot N_2$ (ca. 30% conversion to $4 \cdot N_2$ after 3 days in solution under an N_2 atmosphere). Removal of the N_2 atmosphere by subjecting a solution of **4** and $4 \cdot N_2$ to sequential freeze–pump–thaw cycles did not lead to regeneration of **4**.

Complex **4** features distorted square pyramidal coordination geometry in the solid state, on the basis of X-ray diffraction analysis, such that the silyl donor occupies the axial position (Figure 3). The Si–Fe–H1 angle of $75(2)^\circ$ is acute, and the

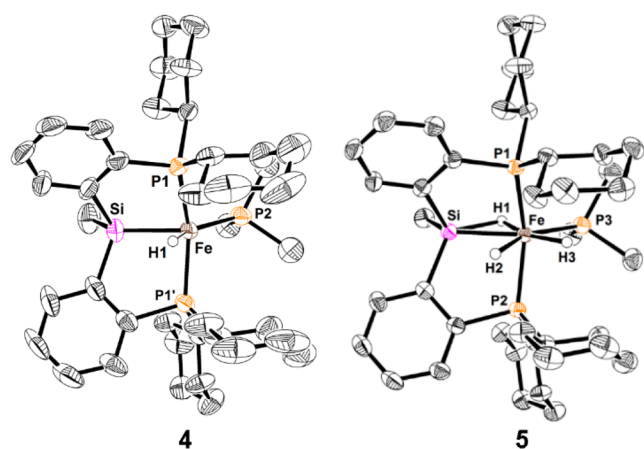


Figure 3. Crystallographically determined structures of **4** (left) and **5** (right) with thermal ellipsoids shown at the 50% probability level; hydrogen atoms not coordinated to Fe have been omitted for clarity. Selected interatomic distances (Å) and angles (deg): for **4** Fe–P1 2.2081(10), Fe–P2 2.2044(18), Fe–Si 2.2727(17), Fe–H1 1.43(6), P1–Fe–P1' 146.98(7), P2–Fe–Si 128.08(8), P2–Fe–H1 157(2), Si–Fe–H1 75(2); for **5** (one of two crystallographically independent molecules) Fe–P1 2.2034(8), Fe–P2 2.1984(8), Fe–P3 2.2053(8), Fe–Si 2.2806(8), Fe–H1 1.49(4), Fe–H2 1.57(3), Fe–H3 1.54(4), P1–Fe–P2 147.56(3), P3–Fe–Si 129.01(3), Si–Fe–H1 50.7(14), Si–Fe–H2 69.6(13), H2–Fe–H3 83.9(19).

Si···H1 distance of ca. 2.48 Å is less than the sum of the van der Waals radii for these atoms (3.4 Å). However, the J_{SiH} value of 19 Hz obtained for **4** falls within a range where it is not possible to make a definitive assignment of η^2 -(Si–H) coordination (while accepted values of J_{SiH} for η^2 -silane complexes range from ca. 40–70 Hz, lower values are possible in some circumstances).³⁰ The solid state structure of the related complex (Cy-PSiP^{Me})Ru(PM_e_3)H has previously been reported²⁷ and features similar coordination geometry. Interestingly, single crystal X-ray analysis of material obtained from treatment of **3** with HBPIn revealed cocrystallized **4** (87.5%) and $4 \cdot N_2$ (12.5%), further substantiating the viability of both iron hydride species (Figure S2 in the Supporting Information).

Surprisingly, mixtures of **4** and $4 \cdot N_2$ were found to react further upon standing in benzene solution (Scheme 2), to generate a third diamagnetic iron hydride species **5**, which

features broad 1H NMR resonances at -9.4 , -9.7 , and -14.6 ppm (1:1:1 ratio). While full conversion to this product was not observed directly from **4** or $4 \cdot N_2$ (ca. 10% conversion to **5** after 3 days), treatment of a mixture of **4** and trace $4 \cdot N_2$ with H_2 (1 atm) led to quantitative (by ^{31}P NMR) formation of **5** after heating at $65^\circ C$ for 18 h. X-ray crystallographic analysis of **5** revealed an apparent η^2 -(Si–H) complex of an Fe(II) dihydride (Figure 3).

Complex **5** adopts distorted octahedral geometry in the solid state, featuring *mer*- κ^3 -coordination of the PSiP ligand. The Fe–Si distance of 2.2806(8) Å is well within the range of 2.2472(4) – 2.2844(4) Å observed for all (Cy-PSiP^{Me})Fe-hydride complexes reported in this work. The acute Si–Fe–H1 angle of $50.7(14)^\circ$ is consistent with a likely interaction between Si and H1. The measured Si···H1 distance of ca. 1.73 Å is much less than the sum of the van der Waals radii of the two atoms (3.4 Å), strongly supporting an Si–H interaction in the solid state. The Si···H2 distance of 2.34 Å, while also less than the sum of the van der Waals radii of Si and H, is significantly longer than the Si···H1 distance. Based on these metrical parameters **5** can be formulated as an η^2 -(Si–H) complex (through Si–H1–Fe) of an Fe dihydride, with a potential secondary interaction between Si and H2 based on their proximity.³¹

In solution, each of H1, H2, and H3 (as labeled in Figure 3) exist in unique environments, as evidenced by three unique Fe–H 1H NMR resonances (a complex multiplet centered at -9.7 ppm and two broad multiplet resonances centered at -9.4 and -14.6 ppm, respectively; a detailed discussion of assignments for these resonances and additional NMR data for **5** can be found in the Supporting Information). At room temperature, selective 1D NOESY experiments (0.5 s mixing time, Figure S6C) indicate exchange between all three hydride environments. The resonance at -9.7 ppm ($J_{SiH} = 65$ Hz) was assigned as H1 on the basis of a 1H – ^{29}Si HMQC experiment (^{29}Si chemical shift: 32.7 ppm). No correlation between Si and either H2 or H3 was observed using 1H – ^{29}Si HMQC or 1H – ^{29}Si HMBC NMR techniques. While there can be considerable ambiguity in the assignment of Si–H–M non-classical interactions,^{30c} the value of 65 Hz for J_{SiH} is consistent with a possible η^2 -(Si–H) interaction in **5** that persists in solution.

Due to the relatively broad nature of the Fe–H resonances in **5** at room temperature, variable temperature 1H NMR experiments were carried out. Upon cooling (Figure S3), the signals in the hydride region of the 1H NMR spectrum gradually sharpened, with the best resolved coupling observed at 253 K. Cooling below this temperature did not lead to further resolution and line shape patterns generally remained consistent between 193 and 273 K. At higher temperatures (Figure S4), the broadened resonances begin to coalesce, with the signals corresponding to H2 and H3 coalescing at approximately 343 K. The signal for H1 also broadens significantly with increasing temperature, but no coalescence was observed up to 353 K.

Overall, the solution state structure of **5** appears to be generally consistent with the solid state structure determined through X-ray crystallographic analysis. Sabo-Étienne³¹ has previously described the importance of secondary interactions in silane complexes of ruthenium and has noted that Si–H distances between 1.9–2.4 Å may indicate the presence of a SISHA (secondary interaction between a silicon and a hydrogen atom). Thus, as the Si–H2 distance of 2.27 Å falls

within this range, the presence of such an interaction cannot be discounted, though no through-bond coupling could be measured between Si and H₂. Measurement of ν_{FeH} and ν_{SiH} values by infrared spectroscopy has been cited as a useful tool for the determination of the presence of a nonclassical interaction, and for **5** ν_{MH} values of 1925 cm⁻¹, 1871 cm⁻¹, and 1846 cm⁻¹ were obtained. Unfortunately as the hydride positions cannot be selectively deuterated (rapid exchange occurs, *vide infra*), values of isotopically shifted IR stretches are of limited value. Sabo-Étienne³¹ cites the presence of a broad and intense IR band in the range 1650–1800 cm⁻¹ as a good indicator of the presence of a σ -(Si–H)-type interaction; however, none of the values for **5** lie within this range. While the IR band at 1846 cm⁻¹ is indeed intense and quite broad, it cannot be definitively assigned as corresponding to a σ -(Si–H).

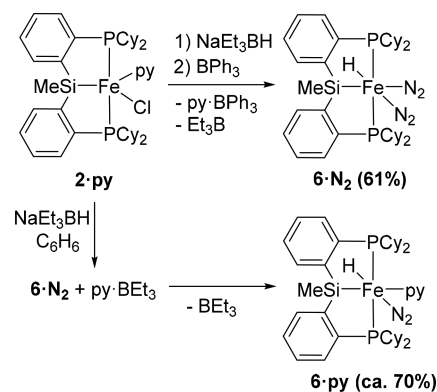
A related Fe-based comparison to **5** is perhaps that of [(PhBP^{iPr}₃)Fe(H)(η^3 -H₂SiRR')] (R = Me; R' = Ph or Mes; PhBP^{iPr}₃ = PhB(CH₂P^{iPr}Pr₂)₃), which as the formula implies has been assigned as an η^3 -silane Fe(II) adduct by Peters and co-workers (binding of the silane through two H atoms, and Si, to the Fe center).³² The bonding scenario for **5** differs significantly, however, in that the Si–H–Fe interaction in **5** involves a tertiary silane and the metal coordination sphere does not feature a similar phosphino-borate component. The Si–H distances in Peters' complexes (1.464(1) and 1.552(2) Å) are both very reasonable for a significant Si–H interaction, while in **5** the Si–H₂ distance of *ca.* 2.27 Å is considerably elongated by comparison and more in line with a SISHA. Furthermore, the ²⁹Si chemical shift of the η^3 -H₂SiRR'–Fe complex is 162 ppm (for R' = Ph), which is dramatically downfield relative to the 32.7 ppm value measured for **5**, a feature cited by Peters as reflective of the η^3 nature of the silane ligand. As such, complex **5** is likely best described as an η^2 -silane adduct of an Fe(II) dihydride. While an Fe(IV) silyl trihydride formulation may also be invoked for **5**, this high oxidation state would be unusual for a 3d metal. The closely related complex Fe(H)₂(H₂)(PEtPh₂)₃ has been unambiguously characterized as an Fe(II)-dihydride dihydrogen adduct that features a similar *cis*-dihydride *mer*-tris(phosphine) coordination geometry to **5**³³ and is likely the most closely matched comparison to the present study.

Complex **5** is a remarkably stable compound, showing little to no evidence of thermal degradation upon extended periods of heating (days, 80 °C) and also appears to be at least moderately air and moisture stable. No reaction of **5** was observed upon addition of CO₂, and no alkene isomerization was observed upon addition of 1-octene. Addition of BPh₃ to **5** did not lead to any apparent generation of Ph₃B·PMe₃, suggesting that PMe₃ does not dissociate readily from the Fe center. However, all three hydride positions in **5** undergo exchange with D₂ (1 atm) to generate **5-d₃**. This exchange is relatively slow at room temperature (no ²H incorporation after 2 h at room temperature, by ¹H NMR) but can be accelerated with heating to 65 °C. From a mechanistic perspective, Sabo-Étienne and co-workers³⁴ have shown that in the case of Ru(H)₂[(η^2 -H-SiMe₂)CH₂CH₂(η^2 -H-SiMe₂)](PCy₃)₂, which features two classical dihydride ligands and two η^2 -(Si–H) interactions, facile exchange of all M–H occurs via a process involving equilibria between the parent structure and isomers that feature, in turn, one dihydrogen ligand, one η^2 -(Si–H) ligand, and a classical silyl group, or two dihydrogen ligands and two classical silyl groups. A similar process involving an

intermediate that features a classical silyl group and a dihydrogen ligand can be invoked for hydride exchange in **5**.

Fe(II)-Hydride Complexes Lacking Exogenous Phosphine Coordination. In an effort to access increasingly reactive iron hydride species, we targeted hydride complexes that did not feature PMe₃ stabilization. Toward this end, treatment of (Cy-PSiP^{Me})H with py₄FeCl₂ and one equiv of BnMgCl was found to generate (Cy-PSiP^{Me})Fe(py)Cl (**2·py**). Treatment of **2·py** with one equiv of NaEt₃BH (Scheme 3) led

Scheme 3. Synthesis of Fe(II)-Hydride Complexes Lacking Exogenous Phosphine Coordination



to the clean (by ³¹P and ¹H NMR) formation of a single diamagnetic product (**6·N₂**), featuring a ³¹P{¹H} NMR resonance at 87.3 ppm, as well as an Fe–H ¹H NMR resonance at –16.31 ppm (t, 1 H, ²J_{PH} = 58.5 Hz). Unexpectedly, upon attempted isolation of this hydride species, partial conversion to a new diamagnetic iron hydride (**6·py**) was observed. This newly formed hydride complex gives rise to a ³¹P{¹H} NMR resonance at 80.2 ppm and an Fe–H ¹H NMR resonance centered at –15.35 ppm (t, 1 H, ²J_{PH} = 60.3 Hz). We suspect that the reversible formation of a pyridine-triethylborane adduct is implicated in this unusual interconversion. Upon attempted workup of the initially generated hydride complex **6·N₂**, the py·BEt₃ byproduct partially dissociates, allowing pyridine to re-coordinate to the Fe center. Exposure of the reaction mixture to vacuum leads to removal of free BEt₃ and drives the conversion of **6·N₂** to the pyridine adduct **6·py**. To circumvent this process, we considered that a more Lewis acidic borane might better sequester pyridine and facilitate the isolation of **6·N₂**. Indeed, addition of one equiv of BPh₃ to the reaction mixture after the addition of NaEt₃BH (Scheme 3) was sufficient to trap pyridine as a py·BPh₃ adduct, allowing for the isolation of **6·N₂**. X-ray crystallographic analysis of both iron hydrides revealed six-coordinate complexes in both cases, where **6·N₂** features two mutually *cis*-N₂ ligands, while **6·py** features one N₂ ligand and one pyridine coordinated to (Cy-PSiP^{Me})FeH.

Both **6·py** and **6·N₂** feature a distorted octahedral geometry in the solid state with κ^3 -coordination of the PSiP ligand in a *mer*-configuration (Figure 4). In each complex the hydride ligand occupies a coordination site *cis* to Si, with acute Si–Fe–H(1) angles of 75.8(7)° and 78.8(7)° for **6·py** and **6·N₂**, respectively. The Si···H(1) distances of *ca.* 2.35 and 2.44 Å (for **6·py** and **6·N₂**, respectively) are both less than the sum of the van der Waals radii for the two atoms, and the measured values of *J*_{SiH} for the two complexes (67 and 70 Hz, respectively) are somewhat high for typical values of ²J_{SiH} for classical *cis*-

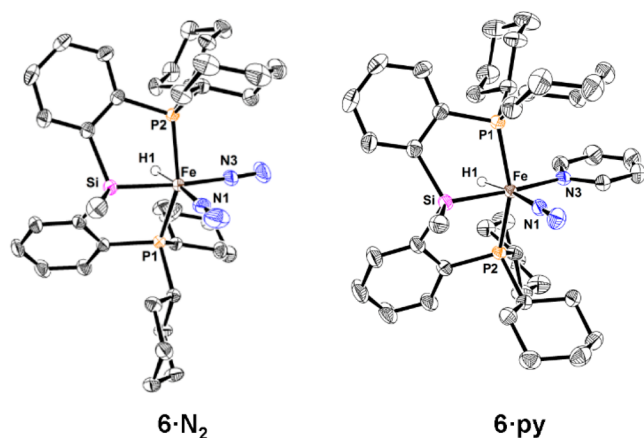


Figure 4. Crystallographically determined structures of **6·N₂** (left) and **6·py** (right) with thermal ellipsoids shown at the 50% probability level; hydrogen atoms not coordinated to Fe have been omitted for clarity. Selected interatomic distances (Å) and angles (deg): for **6·N₂**, Fe–H1 1.418(19), Fe–P1 2.22268(3), Fe–P2 2.2147(3), Fe–Si 2.2844(4), Fe–N1 1.8368(12), Fe–N3 1.8654(12), N1–N2 1.1111(18), N3–N4 1.1065(18), P1–Fe–P2 149.831(13), Si–Fe–N3 174.21(4), N1–Fe–H1 171.4(7), Si–Fe–H1 78.8(7); for **6·py**, Fe–H1 1.441(18), Fe–P1 2.2238(3), Fe–P2 2.2196(3), Fe–Si 2.2472(4), Fe–N1 1.7949(11), Fe–N3 2.0664(11), N1–N2 1.1228(16), P1–Fe–P2 156.068(14), Si–Fe–N3 171.52(3), N1–Fe–H1 168.6(7), Si–Fe–H1 75.8(7).

disposed silyl hydrides, indicating the potential for nonclassical interactions between H and Si in these complexes. Conversely, the ²⁹Si chemical shifts are shifted downfield, to 72.3 and 69.0 ppm, respectively, which are more characteristic of a metal silyl complex rather than, for example, an η²-silane. Further support for the assignment of these complexes as silyl hydrides is provided by infrared spectroscopy, where values of 1949 and 2012 cm⁻¹ for νFeH were measured for **6·py** and **6·N₂**, respectively, neither of which are typical of a nonclassical Si–H interaction.³¹

Both complexes feature an N₂ ligand coordinated *trans* to the Fe–H. The N₂ ligand in **6·py** features a N–N bond length of 1.1228(16) Å, and a value of 2012 cm⁻¹ was measured for the N–N stretching frequency by IR spectroscopy, indicating moderate activation. Comparatively in **6·N₂**, the N₂ ligand bound *trans* to Si features a N–N bond distance of 1.1065(18) Å, while the N₂ *trans* to the Fe–H features a comparable bond distance of 1.1111(18) Å. By use of IR spectroscopy, N–N stretching frequencies of 2123 and 2063 cm⁻¹ were measured for **6·N₂**. The propensity of **6·N₂** to recoordinate pyridine, as observed during its preparation, consistently leads to only one isomer of **6·py** with displacement of the N₂ ligand *trans* to Si. Complex **6·N₂** can also be accessed from **2·PMe₃** through an analogous route; however, the concomitant formation of small amounts of **4**, **4·N₂**, and **5** was typically observed, among other byproducts.

Complex **6·N₂** is particularly intriguing, as it can be thought of as a surrogate for the low-coordinate Fe hydride, (Cy-PSiP^{Me})FeH, which does not appear to be isolable under a N₂ atmosphere. The N₂ ligands (particularly the N₂ bound *trans* to Si) are anticipated to be displaced readily by a variety of incoming donors. We considered that **6·N₂** appeared poised for coordination and subsequent insertion of an unsaturated substrate, and thus we turned our attention toward catalytic alkene hydrogenation using **6·N₂** as a precatalyst.

Alkene Hydrogenation Catalyzed by 6·N₂. As described in the Introduction, relatively few examples of homogeneous Fe-catalyzed alkene hydrogenation have been described in the literature, and with two potentially labile N₂ ligands, similar to Chirik's catalysts,^{3f} **6·N₂** is anticipated to readily coordinate incoming substrate molecules. To survey the effectiveness of **6·N₂** as an alkene hydrogenation precatalyst, 1-octene was first investigated as a substrate. Using **6·N₂** at a 5 mol % loading, 1-octene was hydrogenated to *n*-octane in 98% conversion over 4 h (10 atm H₂, room temperature; Table 1, Entry 1). Under 1

Table 1. Hydrogenation of Alkenes Catalyzed by **6·N₂**

entry	substrate	product	conversion (%) ^a
1		<i>n</i> -octane	98 ^b
2		<i>n</i> -octane	>99
3		<i>n</i> -octane	>99
4			93 ^b
5			94
6			>99 (92) ^c
7			>99
8			97

^aConversion on the basis of ¹H NMR integration using 1,3,5-trimethoxybenzene as an internal standard (average of two runs). ^bReaction performed at room temperature. ^cIsolated yield denoted in parentheses.

atm H₂, 5 mol % **6·N₂** was sufficient to afford *n*-octane in 99% conversion over 18 h at room temperature (Table S1, Entry 1), a time that could be decreased to 4 h by heating at 65 °C (Table S1, Entry 2). Lastly, the catalyst loading could be reduced to 0.5 mol %, affording 97% conversion to *n*-octane after heating for 4 h 65 °C (10 atm H₂; Table S1, Entry 3).

Encouraged by these initial results, the substrate scope was expanded to include a variety of substituted alkenes. While moderately elevated temperature (65 °C) and pressure (10 atm H₂) were required to afford high conversion for such substrates, a wide variety of alkenes were found to be active toward hydrogenation. Both *cis*- and *trans*-4-octene were hydrogenated quantitatively (Table 1, Entries 2 and 3), as was *cis*-stilbene (Table 1, Entry 6). For 4-vinylcyclohexene, at 65 °C, both the internal double bond and the vinyl group were reduced, yielding ethylcyclohexane with 94% conversion (Table 1, Entry 5). When this substrate was hydrogenated at

room temperature, the internal double bond was left intact, and 4-ethylcyclohexene could be obtained selectively in 93% conversion (Table 1, Entry 4). A 1,1-disubstituted alkene, α -methylstyrene, was fully converted to cumene (Table 1, Entry 7), and even a trisubstituted alkene, ethylidenecyclohexane, was hydrogenated to ethylcyclohexane in 97% conversion (Table 1, Entry 8).

Although the reaction of (Cy-PSiP^{Me})Fe(PMe₃)(N₂) (**3**) with H₂ afforded an apparent mixture of paramagnetic species (*vide supra*), the reactivity of **3** was tested under alkene hydrogenation conditions. Using the same conditions employed with **6**·N₂ (5 mol % **3**, 10 atm H₂, 65 °C), only 35% conversion of 1-octene and 17% conversion of *trans*-4-octene to *n*-octane were observed, respectively, after 4 h. No isomerization of 1-octene was observed under these conditions. By comparison, the Co analogue (Cy-PSiP^{Me})Co(PMe₃)(N₂) achieved 95% conversion of 1-octene to *n*-octane under comparable reaction conditions.²⁵ As (Cy-PSiP^{Me})FeH(PMe₃)(N₂)_n (**4**, *n* = 0; **4**·N₂, *n* = 1) converts to **5** with the addition of hydrogen (*vide supra*), hydrogenation of *trans*-4-octene using **5** was also attempted for direct comparison with **6**·N₂. Under the typical hydrogenation conditions employed (5 mol % **5**, 10 atm H₂, 65 °C) <5% conversion to *n*-octane was observed after 4 h. Collectively, these observations establish **6**·N₂ as being superior among the bis(phosphino)silyl Fe precatalysts examined herein.

Notably, hydrogenation catalyzed by **6**·N₂ was found to proceed with functional group tolerance toward ester and ether functionalities. Ethyl crotonate was hydrogenated to ethyl butanoate in 80% conversion under the standard conditions (Table 2, Entry 2), while allyl butyl ether and allyl phenyl ether were hydrogenated with 96 and 98% conversions, respectively (Table 2, Entries 3 and 4). Notably for these C–O-containing

substrates, no special precautions were required to prevent undesired C–O bond cleavage chemistry involving the substrate;^{5,9} all substrates were combined with the precatalyst at room temperature prior to introduction of H₂. Ketones appear to not be tolerated by this system, with 11% conversion obtained in the hydrogenation of 5-hexen-2-one (Table 2, Entry 1); no evidence for reduction of the carbonyl was observed. Hydrogenation of a terminal alkyne, phenylacetylene, was also attempted; however, a complex mixture of products was obtained (by ¹H NMR), and while no unreacted phenylacetylene was observed, the only products that could be identified were ethylbenzene (*ca.* 19%) and 1,4-diphenylbutane (*ca.* 14%). The generation of 1,4-diphenylbutane implicates a homocoupling process, followed by hydrogenation. Such a process could yield a variety of hydrogenated or partially hydrogenated derivatives and may in part explain the large product distribution obtained. A 1,2-disubstituted alkyne, diphenylacetylene, was better tolerated by the catalyst, and under standard conditions 36% conversion to bibenzyl was observed, with 42% conversion to *trans*-stilbene (Table 2, Entry 5).³⁵ However, by increasing the temperature to 90 °C and the reaction time to 6 h, selective formation of bibenzyl in 92% conversion was obtained (Table 2, Entry 6).

While (PDI)Fe(N₂)₂ and (CNC)Fe(N₂)₂ alkene hydrogenation catalysts of the type developed by Chirik and co-workers^{5,11b} are apparently more active than **6**·N₂, the latter PSiP complex is notable in that it represents a rare example of an Fe catalyst that is capable of effectively hydrogenating a comparable range of alkene substrates, including aliphatic alkenes and a trisubstituted example, under relatively mild conditions. Moreover, the reactivity of **6**·N₂ is complementary, in that side reactions involving C–O bond cleavage have not been observed, allowing for facile reduction of alkenes that feature ether and ester functionality. Further efforts to fine-tune the PSiP ligand scaffold may lead to increased activity and selectivity, and such strategies are currently being investigated by our group, as are the mechanistic details of these transformations.

Table 2. Hydrogenation of Functionalized Alkenes and Alkynes Catalyzed by **6·N₂**

entry	substrate	product	conversion (%) ^a
1			11
2			80
3			96
4			98
5			42 ^b
6			92 ^c

^aConversion on the basis of ¹H NMR integration using 1,3,5-trimethoxybenzene as an internal standard (average of two runs).

^bConversion to *trans*-stilbene; 36% conversion to bibenzyl also observed; no *cis*-stilbene observed. ^cReaction performed in toluene-*d*₈ for 6 h, at 90 °C.

3. CONCLUSION

Thus far, literature examples of iron complexes supported by phenylene-based PSiP pincer ligation have been limited to only two examples of coordinatively saturated 18-electron complexes of Fe(II).^{2,6a,c} We have expanded the Fe chemistry of this versatile ligand class, providing examples of coordinatively unsaturated Fe(II) and Fe(I) complexes supported by Cy-PSiP^{Me}. While isolable four-coordinate Fe(II) complexes remain elusive, possibly due to their inherent instability toward one-electron redox processes, we have demonstrated that five-coordinate analogues are readily prepared and isolated.

A variety of diamagnetic iron hydride species have been observed and characterized herein, and interconversion among such complexes facilitated by the coordination of N₂ has been documented. We have also observed evidence for η^2 -silane coordination in such iron hydride species involving the PSiP ligand, and such interactions may play a role in the subsequent reactivity of these complexes. A unique example of an η^2 -(Si–H) complex of an Fe dihydride (**5**) was investigated thoroughly by use of a suite of 1D- and 2D-NMR techniques over a range of temperatures to elucidate the probable bonding situation in this complex. We also successfully prepared a PSiP-supported iron hydride complex stabilized only by N₂

coordination ($6 \cdot N_2$), which can be thought of as a surrogate for the unobserved four-coordinate species $(Cy-PSiP^{Me})FeH$. This complex was found to be an effective, easily manipulated precatalyst for the hydrogenation of a range of terminal and multiply substituted alkenes. Esters and ethers were found to be well-tolerated by the catalyst, and alkyne hydrogenation was also demonstrated. This represents a relatively rare example of Fe-catalyzed alkene direct hydrogenation, a reaction of fundamental importance in organometallic catalysis.

4. EXPERIMENTAL SECTION

General Considerations. All experiments were conducted under nitrogen in a glovebox or using standard Schlenk techniques. Tetrahydrofuran and diethyl ether were distilled from Na/benzophenone ketyl. Benzene, toluene, and pentane were first sparged with nitrogen and subsequently dried by passage through a double-column (one activated alumina column and one column packed with activated Q-5) solvent purification system. All purified solvents were stored over 4 Å molecular sieves. Benzene- d_6 and cyclohexane- d_{12} were degassed via three freeze–pump–thaw cycles and stored over 4 Å molecular sieves. The ligand precursor $(Cy-PSiP^{Me})H^{21}$ and $FeCl_2(THF)_{1.5}$ were prepared by previously reported methods. All other reagents were purchased from commercial suppliers and used without further purification. Unless otherwise stated, 1H , ^{13}C , ^{11}B , ^{31}P , and ^{29}Si characterization data were collected at 300 K, with chemical shifts reported in parts per million downfield of $SiMe_4$ (for 1H , ^{13}C , and ^{29}Si), $BF_3 \cdot OEt_2$ (for ^{11}B), or 85% H_3PO_4 in D_2O (for ^{31}P). 1H and ^{13}C NMR chemical shift assignments are based on data obtained from $^{13}C\{^1H\}$, ^{13}C -DEPTQ, 1H - 1H COSY, 1H - ^{13}C HSQC, and 1H - ^{13}C HMBC NMR experiments. ^{29}Si NMR assignments are based on 1H - ^{29}Si HMBC and 1H - ^{29}Si HMQC experiments. Solution magnetic moment measurements were determined by use of the Evans method.³⁷ Infrared spectra were recorded as thin films between NaCl plates at a resolution of 4 cm^{-1} .

$(Cy-PSiP^{Me})Fe(PMe_3)Cl$ ($2 \cdot PMe_3$). A solution of $(Cy-PSiP^{Me})H$ (0.25 g, 0.42 mmol) in ca. 3 mL of THF was added to a suspension of $FeCl_2(THF)_{1.5}$ (0.099 g, 0.42 mmol) in ca. 3 mL of THF. Neat PMe_3 (0.064 g, 0.85 mmol) was added to the resulting suspension. The reaction mixture was stirred at room temperature until all solids were dissolved to give a green solution (ca. 2–3 min). The reaction mixture was subsequently cooled to $-35\text{ }^\circ\text{C}$, and $BnMgCl$ (0.30 mL, 1.4 M in THF, 0.42 mmol) was added dropwise. The resulting red solution was stirred for 2 h at room temperature, at which point the volatile components were removed under vacuum. The resulting residue was extracted with ca. 5 mL benzene and filtered through Celite. The filtrate solution was evaporated to dryness, and the remaining residue was triturated with $3 \times 5\text{ mL}$ of pentane to afford paramagnetic $2 \cdot PMe_3$ (0.30 g, 94% yield) as a red-orange solid. Crystals of $2 \cdot PMe_3$ suitable for X-ray diffraction analysis were obtained from a concentrated Et_2O solution at $-35\text{ }^\circ\text{C}$. μ_{eff} (benzene- d_6): $3.04\ \mu_B$ ($S = 1$). 1H NMR (benzene- d_6 , 300 MHz) δ : 73.65, 62.73, 22.18, 6.56, 6.24, 5.29, 4.67, 3.90, -0.40 – -2.10 (overlapping resonances), -1.43 , -2.32 , -3.39 , -6.76 , -51.01 . Anal. Calcd for $C_{40}H_{64}P_3SiClFe$: C, 63.44; H, 8.52. Found: C, 63.08; H, 8.74.

$(Cy-PSiP^{Me})Fe(CO)_2Cl$ ($2 \cdot (CO)_2$). *Method 1.* A 250 mL resealable Schlenk flask equipped with a Teflon stopcock and containing a magnetic stirrer was charged with a $FeCl_2(THF)_{1.5}$ (0.099 g, 0.42 mmol). A solution of $(Cy-PSiP^{Me})H$ (0.25 g, 0.42 mmol) in ca. 10 mL THF was added. The reaction mixture was degassed through three sequential freeze–pump–thaw cycles and then placed under an atmosphere of CO. The mixture was then cooled to $0\text{ }^\circ\text{C}$, and a solution of $BnMgCl$ (0.30 mL, 1.4 M in THF, 0.42 mmol) in ca. 2 mL of THF was added dropwise via syringe under a flow of CO, resulting in a gradual color change to green-yellow. The reaction mixture was allowed to warm to room temperature and stir for 2 days under a static CO atmosphere. The volatile components of the reaction mixture were subsequently removed *in vacuo*, and the resulting residue was triturated with $3 \times 2\text{ mL}$ pentane and extracted with 5 mL

benzene and filtered through Celite. The filtrate solution was collected, and benzene was removed *in vacuo*. The remaining residue was triturated with $3 \times 2\text{ mL}$ pentane and washed with $3 \times 1\text{ mL}$ cold ($-35\text{ }^\circ\text{C}$) Et_2O to afford $2 \cdot (CO)_2$ as a tan solid (0.18 g, 58% yield). *Method 2:* A 250 mL resealable Schlenk flask equipped with a Teflon stopcock was charged with a solution of $2 \cdot PMe_3$ (0.10 g, 0.13 mmol) in ca. 7 mL of THF. The solution was degassed via three freeze–pump–thaw cycles and then placed under an atmosphere of CO. A color change from red-orange to light orange was observed in under 1 min. After stirring for a further 10 min, the volatile components of the reaction mixture were removed *in vacuo*. The remaining residue was triturated with ca. 2 mL of pentane and subsequently washed with $3 \times 2\text{ mL}$ of pentane to afford $2 \cdot (CO)_2$ (0.081 g, 84% yield) as a tan solid. X-ray quality crystals of $2 \cdot (CO)_2$ were obtained from a concentrated Et_2O solution $-35\text{ }^\circ\text{C}$. 1H NMR (300 MHz, benzene- d_6): δ 8.13 (d, $J = 7\text{ Hz}$, 2 H, H_{arom}), 7.47 (m, 2 H, H_{arom}), 7.27–7.15 (4 H, H_{arom}), 2.61–2.55 (6 H, PCy), 2.20–1.95 (8 H, PCy), 1.80–1.05 (30 H, PCy), 0.95 (s, 3 H, $SiMe$). ^{13}C NMR (75.5 MHz, benzene- d_6): δ 218.1 (Fe-CO), 212.2 (Fe-CO), 156.6 (apparent t, $J = 21\text{ Hz}$, C_{arom}), 142.5 (apparent t, $J = 24\text{ Hz}$, C_{arom}), 133.7 (apparent t, $J = 9\text{ Hz}$, CH_{arom}), 131.0 (CH_{arom}), 129.4 (CH_{arom}), 127.6 (CH_{arom}), 42.8 (apparent t, $J = 9\text{ Hz}$, CH_{Cy}), 41.4 (apparent t, $J = 10\text{ Hz}$, CH_{Cy}), 33.6 ($CH_{2\text{Cy}}$), 29.9 ($CH_{2\text{Cy}}$), 29.0–28.8 (overlapping resonances, $CH_{2\text{Cy}}$), 28.2 ($CH_{2\text{Cy}}$), 27.7 ($CH_{2\text{Cy}}$), 27.3 ($CH_{2\text{Cy}}$), 26.6 ($CH_{2\text{Cy}}$), 26.3 ($CH_{2\text{Cy}}$), 9.2 ($SiMe$). $^{31}P\{^1H\}$ NMR (121.5 MHz, benzene- d_6): δ 86.2. ^{29}Si NMR (59.6 MHz, benzene- d_6): δ 64.3. IR (thin film, cm^{-1}): 1969 (s, ν_{CO}), 1909 (s, ν_{CO}). Anal. Calcd for $C_{39}H_{55}O_2P_2SiClFe$: C, 63.54; H, 7.52. Found: C, 63.29; H, 7.87.

$(Cy-PSiP^{Me})Fe(PMe_3)N_2$ (3**).** Mg powder (0.027 g, 1.1 mmol) was added to a solution of $2 \cdot PMe_3$ (0.085 g, 0.11 mmol) in ca. 5 mL THF. The resulting mixture was stirred for 18 h at room temperature and was subsequently filtered through Celite. The filtrate solution was evaporated to dryness *in vacuo*, and the remaining residue was extracted with pentane (5 mL) and filtered through Celite. The filtrate was collected, and the volatile components were removed *in vacuo*. The resulting red solid was washed with Et_2O ($5 \times 0.25\text{ mL}$) and dried under vacuum to afford paramagnetic **3** (0.052 g, 61% yield) as a bright yellow solid. Crystals of **3** suitable for X-ray diffraction analysis were obtained from a concentrated Et_2O solution at $-35\text{ }^\circ\text{C}$. μ_{eff} (benzene- d_6): $1.88\ \mu_B$ ($S = 1/2$). 1H NMR (300 MHz, benzene- d_6): δ 9.00, 8.20, 8.07, 7.66, 7.32, 7.22, 6.81, 5.68, 5.09, 4.41, 3.85, 3.27, 0.79–2.64 (overlapping resonances). IR (thin film, cm^{-1}): 2011 (s, ν_{N_2}). Anal. Calcd for $C_{40}H_{64}N_2P_3SiFe$: C, 64.07; H, 8.60; N: 3.74. Found: C, 63.75; H, 8.83; N: 3.38.

$(Cy-PSiP^{Me})Fe(PMe_3)H$ (4**).** A solution of $2 \cdot PMe_3$ (0.030 g, 0.040 mmol) in ca. 3 mL benzene was treated with $NaEt_3BH$ (0.040 mL, 1.0 M in toluene, 0.040 mmol) added via microsyringe. A color change from red to dark brown was observed, and the resulting mixture was allowed to stir for 18 h at room temperature. The volatile components of the reaction mixture were removed *in vacuo*, and the remaining residue was triturated with $3 \times 1\text{ mL}$ pentane and extracted with 5 mL of a ca. 1:1 pentane:benzene mixture. The extracts were combined and filtered through a glass microfiber filter. The filtrate solution was evaporated to dryness *in vacuo* and triturated with $3 \times 1\text{ mL}$ pentane to afford **4** as an off-white solid (0.021 g, 74% yield). 1H NMR (500 MHz, benzene- d_6): δ 8.36 (d, $J = 7\text{ Hz}$, 2 H, H_{arom}), 7.01 (d, $J = 8\text{ Hz}$, 2 H, H_{arom}), 7.33 (apparent t, $J = 7\text{ Hz}$, 2 H, H_{arom}), 7.23 (apparent t, $J = 7\text{ Hz}$, 2 H, H_{arom}), 2.38 (m, 2 H, PCy), 2.16 (m, 4 H, PCy), 2.04 (m, 2 H, PCy), 1.05–1.90 (overlapping resonances, 45 H, $PCy + PMe_3$); the PMe_3 resonance was identified as a doublet ($^2J_{\text{PH}} = 6\text{ Hz}$) at 1.49 ppm), 0.96 (s, 3 H, $SiMe$), -18.53 (td, $^2J_{\text{PH}} = 64\text{ Hz}$, $^2J_{\text{PH}} = 24\text{ Hz}$, 1 H, FeH). ^{13}C NMR (125.8 MHz, benzene- d_6): δ 160.5 (apparent t, $J = 21\text{ Hz}$, C_{arom}), 149.6 (m, C_{arom}), 132.0 (apparent t, $J = 8\text{ Hz}$, CH_{arom}), 128.5 (CH_{arom}), 128.4 (CH_{arom}), 127.0 (CH_{arom}), 42.5 (CH_{Cy}), 32.0 (CH_{Cy}), 29.9 ($CH_{2\text{Cy}}$), 29.6 ($CH_{2\text{Cy}}$), 29.1 ($CH_{2\text{Cy}}$), 28.8 ($CH_{2\text{Cy}}$), 28.6–26.6 (overlapping resonances, $CH_{2\text{Cy}}$), 24.3 (d, $^1J_{\text{CP}} = 16\text{ Hz}$, PMe_3), 6.2 ($SiMe$). $^{31}P\{^1H\}$ NMR (202.5 MHz, benzene- d_6): δ 90.0 (d, $^2J_{\text{PP}} = 55\text{ Hz}$, 2 P, $PSiP$), 3.6 (t, $^2J_{\text{PP}} = 55\text{ Hz}$, 1 P, PMe_3). ^{29}Si NMR (99.4 MHz, benzene- d_6): δ 77.4 (d, $J_{\text{SiH}} = 19.5\text{ Hz}$). IR (thin film, cm^{-1}): 1815 (m, ν_{FeH}). This complex was

observed to convert to both $(\text{Cy-PSiP}^{\text{Me}})\text{FeH}(\text{PMe}_3)(\text{N}_2)$ (**4**· N_2)^{26c} and **5** over time (as described fully in the text; Scheme 2), both in the solid state and in solution. As such, satisfactory combustion analysis could not be obtained.

[Cy-PSi(μ -H)P^{Me}]FeH₂(PMe₃) (5). A solution of **2**·PMe₃ (0.067 g, 0.089 mmol) in ca. 5 mL of benzene was treated with NaEt₃BH (0.089 mL, 1.0 M in toluene, 0.089 mmol) added via microsyringe. The resulting mixture was stirred for 2 h at room temperature and then evaporated to dryness *in vacuo*. The remaining residue was triturated with 3 × 2 mL pentane and was subsequently redissolved in ca. 3 mL benzene and filtered through Celite. The filtrate solution was transferred to a 50 mL thick-walled reaction vessel equipped with a Teflon stopcock and was degassed through three sequential freeze-pump-thaw cycles and placed under an atmosphere of H₂. The reaction mixture was allowed to stir for 18 h at 65 °C. The volatile components of the reaction mixture were then removed *in vacuo*. The remaining residue was triturated with 3 × 2 mL pentane and then washed with 3 × 1 mL pentane to yield **5** as a beige-yellow solid (0.052 g, 81% yield). X-ray quality crystals were grown from a concentrated pentane/THF solution of **5** at room temperature. ¹H NMR (300 MHz, benzene-*d*₆; ABXY₂Z spin system, where Y₂Z = (RPCy₂)₂(PMe₃): δ 8.22 (d, *J* = 6.9 Hz, 2 H, *H*_{arom}), 7.42 (d, *J* = 7 Hz, 2 H, *H*_{arom}), 7.26 (apparent t, *J* = 7.2 Hz, 2 H, *H*_{arom}), 7.12 (apparent t, *J* = 7 Hz, 2 H, *H*_{arom}), 2.53 (m, 2 H, PCy), 2.30–1.05 (overlapping resonances, 50 H, PCy + PMe₃ + SiMe), the PMe₃ resonance was identified as a doublet at 1.36 ppm (²*J*_{PH} = 7 Hz); the SiMe resonance was identified as a singlet at 1.13 ppm, 0.79 (m, 2 H, PCy), 0.42 (m, 2 H, PCy), A = -9.5 ppm (1 H, FeH, ²*J*_{HH} = -9.18 Hz, ²*J*_{HH} = -11.63 Hz, ²*J*_{H-PCy2} = 51.07 Hz, ²*J*_{H-PMe3} = 70.40 Hz), B = -9.8 ppm (1 H, SiHFe, ²*J*_{HH} = -9.18 Hz, ²*J*_{H-PCy2} = 16.42 Hz, ²*J*_{H-PMe3} = 41.07 Hz), X = -14.5 ppm (1 H, FeH, ²*J*_{HH} = -11.63 Hz, ²*J*_{H-PCy2} = 59.36 Hz, ²*J*_{H-PMe3} = 15.31 Hz). ¹³C{¹H} NMR (75.5 MHz, benzene-*d*₆): δ 160.1 (*C*_{arom}), 148.1 (*C*_{arom}), 131.8 (*CH*_{arom}), 127.7 (*CH*_{arom}), 127.3 (*CH*_{arom}), 125.8 (*CH*_{arom}), 39.0 (*CH*_{Cy}), 34.5 (apparent t, *J* = 13.6 Hz, *CH*_{Cy}), 29.6 (*CH*_{2Cy}), 29.1 (*CH*_{2Cy}), 28.4–27.3 (overlapping resonances, *CH*_{2Cy}), 26.7 (*CH*_{2Cy}), 9.13 (SiMe). ³¹P{¹H} NMR (121.5 MHz, benzene-*d*₆): δ 100.8 (d, ²*J*_{PP} = 29 Hz, 2 P, PSiP), 18.7 (t, ²*J*_{PP} = 29 Hz, 1 P, PMe₃). ²⁹Si NMR (59.6 MHz, benzene-*d*₆): δ 32.7. IR (KBr pellet, cm⁻¹): 1925 (ν FeH), 1871 (ν FeH), 1846 (ν FeH). Anal. Calcd For C₄₀H₆₇P₃SiFe: C, 66.28; H, 9.32. Found: C, 65.94; H, 9.21.

Generation of (Cy-PSiP^{Me})FeCl(py) (2·py). To a suspension of (pyridine)₄FeCl₂ (0.15 g, 0.34 mmol) in ca. 15 mL THF was added (Cy-PSiP)H (0.20 g, 0.34 mmol). The yellow suspension was stirred for 1 h at room temperature. BnMgCl (0.24 mL, 0.34 mmol) as a 1.4 M solution in THF was diluted to approximately 2 mL in THF and added dropwise to the stirring suspension at room temperature. A color change from bright yellow to dark red was observed, and the resulting mixture was allowed to stir for 18 h at room temperature. The volatile components of the reaction mixture were removed *in vacuo* and the resulting residue was triturated with 3 × 3 mL pentane and extracted with ca. 10 mL benzene and filtered through Celite. The filtrate solution was collected and solvent was removed *in vacuo*. The residue was triturated with 3 × 3 mL pentane and washed with 3 × 2 mL pentane to afford **2**·py as a red solid (0.21 g, 80% crude yield). We have not been able to obtain satisfactory elemental analysis for this compound. Nonetheless, crude **2**·py, prepared and isolated as described above, was used directly and with success for subsequent syntheses. μ_{eff} (benzene-*d*₆): 2.93 μ_{B} (*S* = 1). ¹H NMR (benzene-*d*₆, 300 MHz): δ 61.15, 42.00, 16.00, 15.97, 10.76, 8.75, 5.66, 5.15, 3.41, 2.50–0.40 (overlapping resonances), -0.19, -0.56, -1.04, -2.96, -3.29, -4.84, -9.68, -61.0.

Generation of (Cy-PSiP^{Me})FeH(py)(N₂) (6·py). A solution of **2**·py (0.037 g, 0.049 mmol) in ca. 3 mL of benzene was treated with NaEt₃BH (0.049 mL, 1.0 M in toluene, 0.049 mmol) added via microsyringe. A gradual color change from dark red-orange to yellow-orange was observed, and the mixture was stirred for 18 h at room temperature. The volatile components of the reaction mixture were removed *in vacuo*, and the remaining residue was triturated with 3 × 2 mL pentane. The residue was then extracted with ca. 3 mL benzene,

and the collected extracts were filtered through Celite, combined with ca. 5 equiv pyridine (20 μ L), and allowed to stir briefly (5 min) before all volatile components were removed *in vacuo*. The resulting solid was triturated with 3 × 2 mL pentane and washed with 3 × 0.5 mL cold (-35 °C) pentane to afford a mixture of **6**·py and **6**·N₂ (0.024 g; ca. 1:1 ratio of **6**·py to **6**·N₂, typically obtained). A slight excess of pyridine was thus added to the mixture to minimize the amount of **6**·N₂ for solution spectroscopic analysis. In one instance, a minute quantity of X-ray quality crystals of **6**·py was obtained from a concentrated Et₂O solution of a mixture of **6**·py and **6**·N₂, as prepared above, at room temperature. ¹H NMR (300 MHz, benzene-*d*₆): δ 9.35 (broad, 1 H, *H*_{py}), 8.31 (d, *J* = 7 Hz, 2 H, *H*_{arom}), 8.14 (broad, 1 H, *H*_{py}), 7.75 (d, *J* = 7 Hz, 2 H, *H*_{arom}), 7.35 (apparent t, *J* = 7 Hz, 2 H, *H*_{arom}), 7.26 (apparent t, *J* = 7 Hz, 2 H, *H*_{arom}), 6.81 (broad, 1 H, *H*_{py}), 6.55–6.30 (overlapping resonances, 2 H, *H*_{py}), 2.62 (m, 2 H, PCy), 2.10–0.90 (overlapping resonances, 42 H, PCy), 0.75 (s, 3 H, SiMe), -15.34 (t, ²*J*_{PH} = 61 Hz, 1 H, FeH). ¹³C{¹H} NMR (125.8 MHz, benzene-*d*₆): δ 162.2 (apparent t, *J* = 23.9 Hz, *C*_{arom}), 159.8 (*CH*_{py}), 153.7 (*CH*_{py}), 147.1 (apparent t, *J* = 25 Hz, *C*_{arom}), 133.4 (*CH*_{py}), 132.6 (t, *J* = 8.8 Hz, *CH*_{arom}), 129.0 (*CH*_{arom}), 128.9 (*CH*_{py}), 128.8 (*CH*_{arom}), 127.2 (*CH*_{arom}), 123.3 (*CH*_{py}), 40.4 (*CH*_{Cy}), 32.3 (*CH*_{Cy}), 29.9 (*CH*_{2Cy}), 29.4 (*CH*_{2Cy}), 29.2 (*CH*_{2Cy}), 28.9 (*CH*_{2Cy}), 28.4–28.1 (overlapping resonances, *CH*_{2Cy}), 28.0 (*CH*_{2Cy}), 27.7 (*CH*_{2Cy}), 27.5 (*CH*_{2Cy}), 27.3 (*CH*_{2Cy}), 6.2 (SiMe). ³¹P{¹H} NMR (121.5 MHz, benzene-*d*₆): δ 80.2. ²⁹Si NMR (99.4 MHz, benzene-*d*₆): δ 72.3 (²*J*_{SiH} = 67 Hz). IR (thin film, cm⁻¹): 2012 (ν N₂), 1949 (ν FeH).

(Cy-PSiP^{Me})FeH(N₂)₂ (6·N₂). A solution of **2**·py (0.11 g, 0.14 mmol) in ca. 7 mL of benzene was treated with NaEt₃BH (0.14 mL, 1.0 M in toluene, 0.14 mmol) added via microsyringe. A gradual color change from dark red-orange to yellow-orange was observed, and the reaction mixture was allowed to stir for 18 h at room temperature. A solution of BPh₃ (0.034 g, 0.14 mmol) in ca. 1 mL benzene was then added, and the reaction mixture was allowed to stir for a further 2 h. The volatile components of the reaction mixture were removed *in vacuo*, and the resulting residue was triturated with 3 × 3 mL pentane and then extracted with ca. 15 mL pentane, and the combined extracts were filtered through Celite. The filtrate solution was evaporated to dryness, and the remaining residue was subsequently washed with 3 × 1 mL pentane to yield **6**·N₂ as a tan solid (0.051 g, 61% yield). X-ray quality crystals were obtained from a concentrated solution of **6**·N₂ in 1:1 pentane: Et₂O at room temperature. ¹H NMR (500 MHz, benzene-*d*₆): δ 8.14 (d, *J* = 7 Hz, 2 H, *H*_{arom}), 7.58 (d, *J* = 7 Hz, 2 H, *H*_{arom}), 7.30 (apparent t, *J* = 7 Hz, 2 H, *H*_{arom}), 7.19 (apparent t, *J* = 7 Hz, 2 H, *H*_{arom}), 2.49 (m, 2 H, PCy), 2.39 (m, 2 H, PCy), 2.23 (m, 2 H, PCy), 2.02 (m, 2 H, PCy), 1.91 (m, 2 H, PCy), 1.86–1.75 (overlapping resonances, 4 H, PCy), 1.70 (m, 2 H, PCy), 1.65–1.46 (overlapping resonances, 12 H, PCy), 1.44–1.04 (overlapping resonances, 16 H, PCy), 0.71 (s, 3 H, SiMe), -16.31 (t, ²*J*_{PH} = 59 Hz, 1 H, FeH). ¹³C NMR (125.8 MHz, benzene-*d*₆): δ 159.9 (apparent t, *J* = 24 Hz, *C*_{arom}), 145.1 (apparent t, *J* = 26 Hz, *C*_{arom}), 132.5 (apparent t, *J* = 9 Hz, *CH*_{arom}), 129.2 (*CH*_{arom}), 128.7 (*CH*_{arom}), 127.4 (*CH*_{arom}), 39.6 (apparent t, *J* = 5 Hz, *CH*_{Cy}), 38.6 (apparent t, *J* = 10 Hz, *CH*_{Cy}), 29.6 (*CH*_{2Cy}), 29.5 (*CH*_{2Cy}), 28.9 (*CH*_{2Cy}), 28.2–28.0 (overlapping resonances, *CH*_{2Cy}), 27.6 (*CH*_{2Cy}), 27.3 (apparent t, *J* = 6 Hz, *CH*_{2Cy}), 27.1 (*CH*_{2Cy}), 26.7 (*CH*_{2Cy}), 5.9 (SiMe). ³¹P NMR (202.5 MHz, benzene-*d*₆): δ 87.3. ²⁹Si NMR (99.4 MHz, benzene-*d*₆): δ 69.0 (d, *J*_{SiH} = 70 Hz). IR (thin film, cm⁻¹): 2123 (ν N₂), 2063 (ν N₂), 2012 (ν FeH). Anal. Calcd for C₃₇H₅₆N₄P₂SiFe: C, 63.24; H, 8.03; N, 7.97. Found: C, 62.91; H, 7.88; N, 7.80.

General Procedure for Catalytic Hydrogenation Experiments. All hydrogenations were performed on a 0.057 mmol substrate scale using a 250 μ L total reaction volume. All substrates and catalysts were delivered via microsyringe as stock solutions in the indicated solvent (typically benzene-*d*₆). A 1 dram vial containing preweighed internal standard (1,3,5-trimethoxybenzene) was charged with 0.057 mmol substrate (as a stock solution in benzene-*d*₆) and **6**·N₂ (as a stock solution in benzene-*d*₆). Additional benzene-*d*₆ was then added to bring the total reaction volume to 250 μ L. The vial was then equipped with a stirbar and closed with a PTFE-sealed cap, with a needle inserted through the seal to allow for introduction of H₂ gas.

The vial was then transferred to a Parr reactor which was sealed and purged with H₂ and subsequently pressurized to 10 atm. The Parr reactor was heated to 65 °C in an oil bath for the duration of the reaction time. Afterward, the Parr reactor was removed from heat, allowed to cool to room temperature, and depressurized of H₂. In the glovebox, the sample was transferred to an NMR tube for data acquisition. For calculation of NMR conversions, a chosen diagnostic product signal was integrated relative to that of the internal standard. An excessively long relaxation delay (60 s) was used to ensure accurate integration. All reactions were performed in duplicate, and reported conversions are the average of both runs. The same procedure was followed for all hydrogenations at 10 atm, with variations in solvent, catalyst, or temperature, as indicated. For hydrogenations at 1 atm (at room temperature or 65 °C), reactions were performed in a 50 mL thick-walled reaction vessel equipped with a Teflon stopcock, from which headspace N₂ was removed via one freeze–pump–thaw cycle.

Procedure for Catalytic Hydrogenation of α -Methylstyrene.

A 1 dram vial containing 1,3,5-trimethoxybenzene (9.7 mg) was charged with 0.057 mmol α -methylstyrene (82.7 μ L of a 0.69 M stock solution in benzene-*d*₆) and 6•N₂ (as 100 μ L of a 0.028 M stock solution in benzene-*d*₆). Benzene-*d*₆ (67.3 μ L) was then added to bring the total reaction volume to 250 μ L. The vial was then equipped with a stirbar and closed with a PTFE-sealed cap, with a needle inserted through the seal to allow for the introduction of H₂ gas. The vial was then transferred to a Parr reactor which was sealed and purged with H₂ and subsequently pressurized to 10 atm. The Parr reactor was heated at 65 °C in an oil bath for 4 h. Afterward, the Parr reactor was removed from heat, allowed to cool to room temperature, and depressurized of H₂. In the glovebox, the sample was transferred to an NMR tube for data acquisition. 98.6% conversion to cumene (0.055 mmol) was calculated relative to the internal standard by ¹H NMR spectroscopy. This value represents one of two runs averaged to give the value reported in Table 1.

Procedure for Catalytic Hydrogenation of *cis*-Stilbene and Isolation of Bibenzyl.

A 1 dram vial was charged with 0.020 g of 6•N₂ (0.028 mmol) and 2.4 mL of benzene. *cis*-Stilbene (102 μ L, 0.57 mmol) was added via microsyringe. The vial was then equipped with a stirbar and closed with a PTFE-sealed cap with a needle inserted through the seal to allow for the introduction of H₂ gas. The vial was then transferred to a Parr reactor which was sealed and purged with H₂ and subsequently pressurized to 10 atm. The Parr reactor was heated at 65 °C in an oil bath for 4 h. Afterward, the Parr reactor was removed from heat, allowed to cool, and depressurized of H₂. In the glovebox, the sample was evaporated to dryness *in vacuo* and the residue was extracted with 3 mL of pentane and filtered through a plug of silica gel. The filtrate solution was concentrated *in vacuo* and cooled to –35 °C. Bibenzyl was isolated as a white crystalline solid (0.095 g, 2 crops, 0.52 mmol by this method).

Crystallographic Solution and Refinement Details.

Crystallographic data were obtained at 173(±2) K on a Bruker D8/APEX II CCD diffractometer using Cu K α (λ = 1.54178 Å, microfocus source) radiation, employing a sample that was mounted in inert oil and transferred to a cold gas stream on the diffractometer. Programs for diffractometer operation, data collection, and data reduction (including SAINT) were supplied by Bruker. Gaussian integration (face-indexed) was employed as the absorption correction method in each case. The structures of 2•PMe₃ and 3 were solved by use of the Patterson search/structure expansion, while those of 2•(CO)₂, 4, 5, 6•py, and 6•N₂ were solved by use of intrinsic phasing methods. All structures were refined by use of full-matrix least-squares procedures (on F²) with R₁ based on F_o² ≥ 2σ(F_o²) and wR₂ based on F_o² ≥ –3σ(F_o²). With some exceptions (see Supporting Information and the deposited CIFs), anisotropic displacement parameters were employed throughout for the non-hydrogen atoms. In the case of 4, 5, 6•py, and 6•N₂, the Fe–H (H1; for 5, H2 and H3 are also included) were located in the difference Fourier map and refined isotropically. All remaining hydrogen atoms were added at calculated positions and refined by use of a riding model employing isotropic displacement parameters based on the isotropic displacement parameter of the

attached atom. Additional crystallographic detail is available in the deposited CIFs (CCDC 1870820–1870830).

■ ASSOCIATED CONTENT

Supporting Information

The Supporting Information is available free of charge on the ACS Publications website at DOI: 10.1021/acs.organomet.8b00807.

Experimental details for synthesis of all complexes and hydrogenation procedures, crystallographic refinement details, supplementary hydrogenation data, detailed discussion and supplementary spectroscopic data for complex 5, and selected NMR spectra for reported complexes and hydrogenation experiments (PDF)

Accession Codes

CCDC 1870820–1870830 contain the supplementary crystallographic data for this paper. These data can be obtained free of charge via www.ccdc.cam.ac.uk/data_request/cif, or by emailing data_request@ccdc.cam.ac.uk, or by contacting The Cambridge Crystallographic Data Centre, 12 Union Road, Cambridge CB2 1EZ, UK; fax: +44 1223 336033.

■ AUTHOR INFORMATION

Corresponding Author

*E-mail for L.T.: laura.turculet@dal.ca.

ORCID

Michael J. Ferguson: 0000-0002-5221-4401

Robert McDonald: 0000-0002-4065-6181

Laura Turculet: 0000-0002-2499-5343

Notes

The authors declare no competing financial interest.

■ ACKNOWLEDGMENTS

We are grateful to the Natural Sciences and Engineering Research Council (NSERC) of Canada, the Killam Trusts, and Dalhousie University for their support of this work.

■ REFERENCES

- (1) (a) *Handbook of Homogeneous Hydrogenation*; de Vries, J. G., Elsevier, C. J., Eds.; Wiley-VCH: Weinheim, 2007. (b) Blaser, H. U.; Malan, C.; Pugin, B.; Spindler, F.; Steiner, H.; Studer, M. Selective Hydrogenation for Fine Chemicals: Recent Trends and New Developments. *Adv. Synth. Catal.* **2003**, *345*, 103–151.
- (2) (a) Chirik, P. J. In *Catalysis Without Precious Metals*; Bullock, R. M., Ed.; Wiley-VCH: Weinheim, 2010; pp 83–110. (b) Junge, K.; Schroder, K.; Beller, M. Homogeneous catalysis using iron complexes: recent developments in selective reductions. *Chem. Commun.* **2011**, *47*, 4849–4859. (c) Le Bailly, B. A. F.; Thomas, S. P. Iron-catalysed reduction of carbonyls and olefins. *RSC Adv.* **2011**, *1*, 1435–1445.
- (3) (a) Knijnenburg, Q.; Horton, A. D.; van der Heijden, H.; Kooistra, T. M.; Hettterscheid, D. G. H.; Smits, J. M. M.; de Bruin, B.; Budzelaar, P. H. M.; Gal, A. W. Olefin hydrogenation using diimine pyridine complexes of Co and Rh. *J. Mol. Catal. A: Chem.* **2005**, *232*, 151–159. (b) Monfette, S.; Turner, Z. R.; Semproni, S. P.; Chirik, P. J. Enantiopure C₁-Symmetric Bis(imino)pyridine Cobalt Complexes for Asymmetric Alkene Hydrogenation. *J. Am. Chem. Soc.* **2012**, *134*, 4561–4564. (c) Friedfeld, M. R.; Shevlin, M.; Hoyt, J. M.; Krska, S. W.; Tudge, M. T.; Chirik, P. J. Cobalt Precursors for High-Throughput Discovery of Base Metal Asymmetric Alkene Hydrogenation Catalysts. *Science* **2013**, *342*, 1076–1080. (d) Yu, R. P.; Darmon, J. M.; Milsmann, C.; Margulieux, G. W.; Stieber, S. C.; DeBeer, S.; Chirik, P. J. Catalytic Hydrogenation Activity and Electronic Structure Determination of Bis(arylimidazol-2-ylidene)pyridine Cobalt Alkyl and Hydride Complexes. *J. Am. Chem. Soc.*

- 2013, 135, 13168–13184. (e) Friedfeld, M. R.; Margulieux, G. W.; Schaefer, B. A.; Chirik, P. J. Bis(phosphine)cobalt Dialkyl Complexes for Directed Catalytic Alkene Hydrogenation. *J. Am. Chem. Soc.* **2014**, 136, 13178–13181. (f) Chirik, P. J. Iron- and Cobalt-Catalyzed Alkene Hydrogenation: Catalysis with Both Redox-Active and Strong Field Ligands. *Acc. Chem. Res.* **2015**, 48, 1687–1695. (g) Zhang, G. Q.; Scott, B. L.; Hanson, S. K. Mild and Homogeneous Cobalt-Catalyzed Hydrogenation of C = C, C = O, and C = N Bonds. *Angew. Chem., Int. Ed.* **2012**, 51, 12102–12106. (h) Lin, T. P.; Peters, J. C. Boryl-Metal Bonds Facilitate Cobalt/Nickel-Catalyzed Olefin Hydrogenation. *J. Am. Chem. Soc.* **2014**, 136, 13672–13683. (i) Tokmic, K.; Markus, C. R.; Zhu, L. Y.; Fout, A. R. Well-Defined Cobalt(I) Dihydrogen Catalyst: Experimental Evidence for a Co(I)/Co(III) Redox Process in Olefin Hydrogenation. *J. Am. Chem. Soc.* **2016**, 138, 11907–11913.
- (4) (a) Enthaler, S.; Junge, K.; Beller, M. Sustainable Metal Catalysis with Iron: From Rust to a Rising Star? *Angew. Chem., Int. Ed.* **2008**, 47, 3317–3321. (b) Bauer, L.; Knolker, H. J. Iron Catalysis in Organic Synthesis. *Chem. Rev.* **2015**, 115, 3170–3387. (c) Fürstner, A. Iron Catalysis in Organic Synthesis: A Critical Assessment of What It Takes To Make This Base Metal a Multitasking Champion. *ACS Cent. Sci.* **2016**, 2, 778–789.
- (5) Bart, S. C.; Lobkovsky, E.; Chirik, P. J. Preparation and Molecular and Electronic Structures of Iron(0) Dinitrogen and Silane Complexes and Their Application to Catalytic Hydrogenation and Hydrosilylation. *J. Am. Chem. Soc.* **2004**, 126, 13794–13807.
- (6) (a) Frankel, E. N.; Emken, E. A.; Peters, H. M.; Davison, V. L.; Butterfield, R. O. Homogeneous Hydrogenation of Methyl Linoleate Catalyzed by Iron Pentacarbonyl. Characterization of Methyl Octadecadienoate-Iron Tricarbonyl Complexes. *J. Org. Chem.* **1964**, 29, 3292–3297. (b) Schroeder, M. A.; Wrighton, M. S. Pentacarbonyliron(0) Photocatalyzed Hydrogenation and Isomerization of Olefins. *J. Am. Chem. Soc.* **1976**, 98, 551–558.
- (7) Daida, E. J.; Peters, J. C. Considering Fe^{II/IV} Redox Processes as Mechanistically Relevant to the Catalytic Hydrogenation of Olefins by [PhBP^{Pr}]₃Fe-H_x Species. *Inorg. Chem.* **2004**, 43, 7474–7485.
- (8) Trovitch, R. J.; Lobkovsky, E.; Bill, E.; Chirik, P. J. Functional Group Tolerance and Substrate Scope in Bis(imino)pyridine Iron Catalyzed Alkene Hydrogenation. *Organometallics* **2008**, 27, 1470–1478.
- (9) Trovitch, R. J.; Lobkovsky, E.; Bouwkamp, M. W.; Chirik, P. J. Carbon-Oxygen Bond Cleavage by Bis(imino)pyridine Iron Compounds: Catalyst Deactivation Pathways and Observation of Acyl C-O Bond Cleavage in Esters. *Organometallics* **2008**, 27, 6264–6278.
- (10) (a) Russell, S. K.; Darmon, J. M.; Lobkovsky, E.; Chirik, P. J. Synthesis of Aryl-Substituted Bis(imino)pyridine Iron Dinitrogen Complexes. *Inorg. Chem.* **2010**, 49, 2782–2792. (b) Wile, B. M.; Trovitch, R. J.; Bart, S. C.; Tondreau, A. M.; Lobkovsky, E.; Milsmann, C.; Bill, E.; Wiegardt, K.; Chirik, P. J. Reduction Chemistry of Aryl- and Alkyl-Substituted Bis(imino)pyridine Iron Dihalide Compounds: Molecular and Electronic Structures of [(PDI)₂Fe] Derivatives. *Inorg. Chem.* **2009**, 48, 4190–4200. (c) Russell, S. K.; Milsmann, C.; Lobkovsky, E.; Weyhermuller, T.; Chirik, P. J. Synthesis, Electronic Structure, and Catalytic Activity of Reduced Bis(aldimino)pyridine Iron Compounds: Experimental Evidence for Ligand Participation. *Inorg. Chem.* **2011**, 50, 3159–3169. (d) Darmon, J. M.; Turner, Z. R.; Lobkovsky, E.; Chirik, P. J. Electronic Effects in 4-Substituted Bis(imino)pyridines and the Corresponding Reduced Iron Compounds. *Organometallics* **2012**, 31, 2275–2285.
- (11) (a) Danopoulos, A. A.; Wright, J. A.; Motherwell, W. B. Molecular N₂ complexes of iron stabilised by N-heterocyclic 'pincer' dicarbene ligands. *Chem. Commun.* **2005**, 784–786. (b) Yu, R. P.; Darmon, J. M.; Hoyt, J. M.; Margulieux, G. W.; Turner, Z. R.; Chirik, P. J. High-Activity Iron Catalysts for the Hydrogenation of Hindered, Unfunctionalized Alkenes. *ACS Catal.* **2012**, 2, 1760–1764. (c) Darmon, J. M.; Yu, R. P.; Semproni, S. P.; Turner, Z. R.; Stieber, S. C. E.; DeBeer, S.; Chirik, P. J. Electronic Structure Determination of Pyridine N-Heterocyclic Carbene Iron Dinitrogen Complexes and Neutral Ligand Derivatives. *Organometallics* **2014**, 33, 5423–5433.
- (12) Xu, R. B.; Chakraborty, S.; Bellows, S. M.; Yuan, H. M.; Cundari, T. R.; Jones, W. D. Iron-Catalyzed Homogeneous Hydrogenation of Alkenes under Mild Conditions by a Stepwise, Bifunctional Mechanism. *ACS Catal.* **2016**, 6, 2127–2135.
- (13) Ott, J. C.; Blasius, C. K.; Wadepohl, H.; Gade, L. H. Synthesis, Characterization, and Reactivity of a High-Spin Iron(II) Hydrido Complex Supported by a PNP Pincer Ligand and Its Application as a Homogenous Catalyst for the Hydrogenation of Alkenes. *Inorg. Chem.* **2018**, 57, 3183–3191.
- (14) Buschelberger, P.; Gartner, D.; Reyes-Rodriguez, E.; Kreyenschmidt, F.; Koszinowski, K.; Jacobi von Wangelin, A.; Wolf, R. Alkene Metalates as Hydrogenation Catalysts. *Chem. - Eur. J.* **2017**, 23, 3139–3151.
- (15) Bhor, M. D.; Panda, A. G.; Jagtap, S. R.; Bhanage, B. M. Hydrogenation of α,β -Unsaturated Carbonyl Compounds Using Recyclable Water-Soluble Fe^{II}/EDTA Complex Catalyst. *Catal. Lett.* **2008**, 124, 157–164.
- (16) Manna, K.; Zhang, T.; Carboni, M.; Abney, C. W.; Lin, W. B. Salicylaldimine-Based Metal-Organic Framework Enabling Highly Active Olefin Hydrogenation with Iron and Cobalt Catalysts. *J. Am. Chem. Soc.* **2014**, 136, 13182–13185.
- (17) Gieshoff, T. N.; Villa, M.; Welther, A.; Plois, M.; Chakraborty, U.; Wolf, R.; Jacobi von Wangelin, A. Iron-catalyzed olefin hydrogenation at 1 bar H₂ with a FeCl₃-LiAlH₄ catalyst. *Green Chem.* **2015**, 17, 1408–1413.
- (18) Gieshoff, T. N.; Chakraborty, U.; Villa, M.; Jacobi von Wangelin, A. Fe clusters. *Angew. Chem.* **2017**, 129, 3639–3643.
- (19) Turculet, L. In *Pincer and Pincer-Type Complexes: Applications in Organic Synthesis and Catalysis*; Szabó, K. J., Wendt, O. F., Eds.; Wiley-VCH: Weinheim, 2014; pp 149–188.
- (20) For other recent studies involving P^{Si}P ligation, see: (a) Takaya, J.; Iwasawa, N. In *Pincer and Pincer-Type Complexes: Applications in Organic Synthesis and Catalysis*; Szabó, K. J., Wendt, O. F., Eds.; Wiley-VCH: Weinheim, 2014; pp 229–248. (b) Bernal, M. J.; Torres, O.; Martin, M.; Sola, E. Reversible Insertion of Carbenes into Ruthenium-Silicon Bonds. *J. Am. Chem. Soc.* **2013**, 135, 19008–19015. (c) Suh, H. W.; Guard, L. M.; Hazari, N. A mechanistic study of allene carboxylation with CO₂ resulting in the development of a Pd(II) pincer complex for the catalytic hydroboration of CO₂. *Chem. Sci.* **2014**, 5, 3859–3872. (d) Takaya, J.; Iwasawa, N. Silyl Ligand Mediated Reversible β -Hydrogen Elimination and Hydrometalation at Palladium. *Chem. - Eur. J.* **2014**, 20, 11812–11819. (e) Whited, M. T.; Deetz, A. M.; Boerma, J. W.; DeRossa, D. E.; Janzen, D. E. Formation of Chlorosilyl Pincer-Type Rhodium Complexes by Multiple Si-H Activations of Bis(phosphine)/Dihydrosilyl Ligands. *Organometallics* **2014**, 33, 5070–5073. (f) Bernal, M. J.; Martin, M.; Sola, E. Allenyl to Alkenylcarbyne Tautomerization at the Ru-Si Bond of Ru(κ P,P,Si) Pincer Complexes. *Organometallics* **2015**, 34, 800–803. (g) Charbonneau, D. J.; Balcells, D.; Hazari, N.; Lant, H. M. C.; Mayer, J. M.; Melvin, P. R.; Mercado, B. Q.; Morris, W. D.; Repisky, M.; Suh, H.-W. Dinitrogen-Facilitated Reversible Formation of a Si-H Bond in a Pincer-Supported Ni Complex. *Organometallics* **2016**, 35, 3154–3162. (h) Kameo, H.; Kawamoto, T.; Sakaki, S.; Bourissou, D.; Nakazawa, H. Transition-Metal-Mediated Cleavage of Fluoro-Silanes under Mild Conditions. *Chem. - Eur. J.* **2016**, 22, 2370–2375. (i) Kim, J.; Kim, Y.; Sinha, I.; Park, K.; Kim, S. H.; Lee, Y. The unusual hydricity of a cobalt bound Si-H moiety. *Chem. Commun.* **2016**, 52, 9367–9370. (j) Whited, M. T.; Deetz, A. M.; Donnell, T. M.; Janzen, D. E. Examining the role of Rh/Si cooperation in alkene hydrogenation by a pincer-type [P₂Si]Rh complex. *Dalton Trans* **2016**, 45, 9758–9761.
- (21) MacLean, D. F.; McDonald, R.; Ferguson, M. J.; Caddell, A. J.; Turculet, L. Room temperature benzene C-H activation by a new [PSiP]Ir pincer complex. *Chem. Commun.* **2008**, 5146–5148.
- (22) Morgan, E.; MacLean, D. F.; McDonald, R.; Turculet, L. Rhodium and Iridium Amido Complexes Supported by Silyl Pincer Ligation: Ammonia N-H Bond Activation by a [PSiP]Ir Complex. *J. Am. Chem. Soc.* **2009**, 131, 14234–14236.

(23) Mitton, S. J.; Turculet, L. Mild Reduction of Carbon Dioxide to Methane with Tertiary Silanes Catalyzed by Platinum and Palladium Silyl Pincer Complexes. *Chem. - Eur. J.* **2012**, *18*, 15258–15262.

(24) Murphy, L. J.; Hollenhorst, H.; McDonald, R.; Ferguson, M.; Lumsden, M. D.; Turculet, L. Selective Ni-Catalyzed Hydroboration of CO₂ to the Formaldehyde Level Enabled by New PSiP Ligation. *Organometallics* **2017**, *36*, 3709–3720.

(25) Murphy, L. J.; Ruddy, A. J.; McDonald, R.; Ferguson, M. J.; Turculet, L. Activation of Molecular Hydrogen and Oxygen by PSiP Complexes of Cobalt. *Eur. J. Inorg. Chem.* **2018**, *2018*, 4481–4493.

(26) (a) Wu, S.; Li, X.; Xiong, Z.; Xu, W.; Lu, Y.; Sun, H. Synthesis and Reactivity of Silyl Iron, Cobalt, and Nickel Complexes Bearing a [PSiP]-Pincer Ligand via Si–H Bond Activation. *Organometallics* **2013**, *32*, 3227–3237. (b) Xiong, Z.; Li, X.; Zhang, S.; Shi, Y.; Sun, H. Synthesis and Reactivity of N-Heterocyclic PSiP Pincer Iron and Cobalt Complexes and Catalytic Application of Cobalt Hydride in Kumada Coupling Reactions. *Organometallics* **2016**, *35*, 357–363. (c) Imayoshi, R.; Nakajima, K.; Takaya, J.; Iwasawa, N.; Nishibayashi, Y. Synthesis and Reactivity of Iron- and Cobalt-Dinitrogen Complexes Bearing PSiP-Type Pincer Ligands toward Nitrogen Fixation. *Eur. J. Inorg. Chem.* **2017**, *2017*, 3769–3778.

(27) MacInnis, M. C.; Ruddy, A. J.; McDonald, R.; Ferguson, M. J.; Turculet, L. Synthesis and characterization of five-coordinate, 16-electron Ru^{II} complexes supported by tridentate bis(phosphino)silyl ligation. *Dalton Trans* **2016**, *45*, 15850–15858.

(28) Mankad, N. P.; Whited, M. T.; Peters, J. C. Terminal Fe^I-N₂ and Fe^{II}-H-C Interactions Supported by Tris(phosphino)silyl Ligands. *Angew. Chem., Int. Ed.* **2007**, *46*, 5768–5771.

(29) Fryzuk, M. D.; Johnson, S. A. The continuing story of dinitrogen activation. *Coord. Chem. Rev.* **2000**, *200*, 379–409.

(30) (a) Nikonov, G. I. Recent Advances in Nonclassical Interligand Si^{III}-H Interactions. *Adv. Organomet. Chem.* **2005**, *53*, 217–309. (b) Corey, J. Y. Reactions of Hydrosilanes with Transition Metal Complexes and Characterization of the Products. *Chem. Rev.* **2011**, *111*, 863–1071. (c) Corey, J. Y. Reactions of Hydrosilanes with Transition Metal Complexes. *Chem. Rev.* **2016**, *116*, 11291–11435.

(31) Lachaize, S.; Sabo-Etienne, S. σ -Silane Ruthenium Complexes: The Crucial Role of Secondary Interactions. *Eur. J. Inorg. Chem.* **2006**, *2006*, 2115–2127.

(32) Thomas, C. M.; Peters, J. C. An η^3 -H₂SiR₂ Adduct of [[PhB(CH₂PiPr₂)₃]Fe^{II}H]. *Angew. Chem., Int. Ed.* **2006**, *45*, 776–780.

(33) (a) Aresta, M.; Giannoccaro, P.; Rossi, M.; Sacco, A. Hydrido-complexes of iron(IV) and iron(II). *Inorg. Chim. Acta* **1971**, *5*, 115–118. (b) Crabtree, R. H.; Hamilton, D. G. Classical (M = Os) and Nonclassical (M = Fe, Ru) Polyhydride Structures for the Complexes MH₄(PR₃)₃. *J. Am. Chem. Soc.* **1986**, *108*, 3124–3125. (c) Vander-sluis, L. S.; Eckert, J.; Eisenstein, O.; Hall, J. H.; Huffman, J. C.; Jackson, S. A.; Koetzle, T. F.; Kubas, G. J.; Vergamini, P. J.; Caulton, K. G. An Attractive "Cis-Effect" of Hydride on Neighbor Ligands: Experimental and Theoretical Studies on the Structure and Intramolecular Rearrangements of Fe(H)₂(η^2 -H₂)(PEtPh₂)₃. *J. Am. Chem. Soc.* **1990**, *112*, 4831–4841.

(34) Atheaux, I.; Delpech, F.; Donnadiou, B.; Sabo-Etienne, S.; Chaudret, B.; Hussein, K.; Barthelat, J. C.; Braun, T.; Duckett, S. B.; Perutz, R. N. Exchange Processes in Complexes with Two Ruthenium (η^2 -Silane) Linkages: Role of the Secondary Interactions between Silicon and Hydrogen Atoms. *Organometallics* **2002**, *21*, 5347–5357.

(35) For an example of Co-catalyzed E-selective alkyne hydrogenation/isomerization, see: Tokmic, K.; Fout, A. R. Alkyne Semihydrogenation with a Well-Defined Nonclassical Co-H₂ Catalyst: A H₂ Spin on Isomerization and E-Selectivity. *J. Am. Chem. Soc.* **2016**, *138*, 13700–13705.

(36) Kern, R. J. Tetrahydrofuran Complexes of Transition Metal Chlorides. *J. Inorg. Nucl. Chem.* **1962**, *24*, 1105–1109.

(37) (a) Evans, D. F. The Determination of the Paramagnetic Susceptibility of Substances in Solution by Nuclear Magnetic Resonance. *J. Chem. Soc.* **1959**, 2003–2005. (b) Bain, G. A.; Berry, J. F. Diamagnetic Corrections and Pascal's Constants. *J. Chem. Educ.* **2008**, *85*, 532–536.